

A generalized Bayesian stochastic block model for microbiome community detection

Kevin C. Lutz ^{1*}, Michael L. Neugent ², Tejasv Bedi ³, Nicole J. De Nisco ^{2,4}, and Qiwei Li ^{3*}

¹Peter O'Donnell Jr. School of Public Health, The University of Texas Southwestern Medical Center, Dallas, Texas, 75390, United States

²Department of Biological Sciences, The University of Texas at Dallas, Richardson, Texas, 75080, United States

³Department of Mathematical Sciences, The University of Texas at Dallas, Richardson, Texas, 75080, United States

⁴Department of Urology, The University of Texas Southwestern Medical Center, Dallas, Texas, 75390, United States

*Address correspondence to: Kevin.Lutz@UTSouthwestern.edu and Qiwei.Li@UTDallas.edu

August 29, 2023

Abstract

Advances in next-generation sequencing technology have enabled the high-throughput profiling of metagenomes and accelerated the microbiome study. Recently, there has been a rise in quantitative studies that aim to decipher the microbiome co-occurrence network and its underlying community structure based on metagenomic sequence data. Uncovering the complex microbiome community structure is essential to understanding the role of the microbiome in disease progression and susceptibility. Taxonomic abundance data generated from metagenomic sequencing technologies are high-dimensional and compositional, suffering from uneven sampling depth, over-dispersion, and zero-inflation. These characteristics often challenge the reliability of the current methods for microbiome community detection. To this end, we propose a Bayesian stochastic block model to study the microbiome co-occurrence network based on the recently developed modified centered-log ratio transformation tailored for microbiome data analysis. Our model allows us to incorporate taxonomic tree information using a Markov random field prior. The model parameters are jointly inferred by using Markov chain Monte Carlo sampling techniques. Our simulation study showed that the proposed approach performs better than competing methods even when taxonomic tree information is non-informative. We applied our approach to a real urinary microbiome dataset from postmenopausal women, the first time the urinary microbiome co-occurrence network structure has been studied. In summary, this statistical methodology provides a new tool for facilitating advanced microbiome studies.

1 Introduction

The term *microbiome* was first introduced by Nobel Laureate Joshua Lederberg [53, 58] and refers to the collective genomes of microorganisms or the microorganisms themselves [88]. Ecological interactions of these microorganisms are important because they affect microbiome function and host health through the formation of complex microbiome communities [6]. Uncovering these relationships is essential to understanding the role of the microbiome in disease progression and susceptibility [36, 83]. For example, microbial interactions in the human gut microbiome have been associated with the progression of several diseases such as colorectal cancer [62], diabetes [45], and inflammatory bowel disease [35]. Hall et al. [36] found evidence that the network of microbes in the human gut microbiome is composed of distinct communities that co-occur and interact with one another. Further, it was found that each community tends to have similar metagenomic functional properties. Thus, uncovering the underlying community structure of a microbiome network is the key to understanding its impact on human health [1]. From this point forward, a network of microbial interactions will be referred to as a *microbiome co-occurrence network*.

Network analysis is a widely used statistical method that infers the complex structure and associations among entities such as persons or microbes [37]. A graphical representation of a network consists of nodes and edges. In microbiome research, each node is a taxon and an existing edge represents a significant association between two

taxa. An inferred microbiome co-occurrence network can help characterize taxon-taxon associations and reveal their latent properties, mechanisms, and structures [42]. Co-occurrence research within microbiomes usually considers taxon-taxon associations, which means all microbes are from the same level of the taxonomic tree hierarchy [61]. Network analysis methods use either a similarity metric or a model-based approach to determine these associations. For further information, Lutz et al. [61] provide a detailed survey of available methods for microbiome network analysis.

Community detection is one of the fundamental problems in network analysis. The most widely used model-based approach for performing community detection is the *stochastic block model* (SBM) [46], which was first introduced by Holland et al. [39]. SBM has been employed in a broad range of applications including medicine [57], social media [97], sociology [66], political science [51], military strategy [72], infrastructure [96], and many more. Applications in microbiome co-occurrence networks of bacteria, genes, or proteins include microbial communities associated with pH in arctic soil [29], taxon-taxon communities of the human gut microbiome associated with disease development [63, 36], protein-protein interactions associated with pancreatic cancer [85], optimizing treatment plant operations by understanding microbial communities in wastewater [26], controlling tick-related diseases by understanding the interactions of tick-borne microbial communities over time [56], and the use of protein-protein communities related to SARS-CoV-2 to better understand COVID-19 [32]. Applications using frequentist [51, 2, 97, 85] and Bayesian [66, 28, 36, 70] approaches are available in the literature. Recently, SBMs have been used to uncover the underlying microbiome community structure by clustering all taxa in the microbiome co-occurrence network based on their connectivity patterns [36, 16, 13]. In general, SBMs aim to partition the nodes (e.g., taxa) of a network with heterogeneous connectivity patterns into mutually exclusive blocks (e.g., communities) with homogeneous connectivity patterns [66, 4, 54]. Furthermore, SBMs can infer the latent underlying structural patterns of a network [54] and estimate the edge probabilities within each block and between blocks [4]. Table 3 in the appendix provides a non-exhaustive catalog of available SBM software package information for users in R, Python, and C++, while Table 4 lists the websites for software access and documentation.

We searched the literature for SBMs applied specifically to microbiome co-occurrence network analysis [36, 13, 3, 27, 50, 85, 22, 91, 90], and found that all taxa in the network were from only one level of the taxonomic tree hierarchy (e.g., species). Thus, none of them account for taxonomic tree structure. Integrating the available taxonomic or phylogenetic tree structure into SBMs could provide additional information about microbiome communities because taxa (e.g., species) having the same parent (e.g., genus) or with similar functional properties tend to cluster together [36, 92, 74, 93]. In addition, most of those SBMs ignore multiple characteristics of taxonomic abundance data generated from metagenomic sequencing technology [25], such as high-dimensionality, zero-inflation, over-dispersion, and compositionality [7, 44], resulting in information loss and inference bias [76]. Thus, tailored statistical methods accounting for those challenging characteristics are required.

This paper proposes a generalized Bayesian SBM with a Markov random field (MRF) prior, which we refer to as Bayesian-SBM-MRF. The MRF prior accounts for taxonomic tree structure by allowing the model to incorporate more than one level of the taxonomic tree, which is an attractive and novel feature of our proposed model. Our proposed model considers two sources of binary information to perform microbiome community detection: (i) the taxon-taxon microbiome co-occurrence network and (ii) taxonomic tree information. Unlike other SBMs in the literature for microbiome study, our model applies the recently developed modified centered-log ratio (MCLR) transformation [94] to account for zero-inflation and compositionality in the taxonomic abundance data. Additionally, we use the Spearman correlation coefficient of the MCLR-transformed abundances to identify non-linear pairwise taxon-taxon associations. We show in our simulations that Bayesian-SBM-MRF performs at least as good if not better when we incorporate both (i) and (ii) instead of just only (i) in the analysis, and significantly outperforms other existing SBMs. We implement our model on a real urinary microbiome dataset taken from a controlled, cross-sectional study of recurrent urinary tract infections (rUTI) from post-menopausal women. Additionally, this is the first time that the urinary microbiome community structure has been investigated. We also implemented our model on a second real dataset based on the characters in the classic novel *Les Misérables* to demonstrate its broad use. Our model provides a new tool for advanced studies of microbiome co-occurrence networks.

The remainder of the article is organized as follows: Sections 2 and 3 introduce the data preprocessing, the standard Bayesian SBM, and the proposed generalized SBM with an MRF prior; Section 4 describes the Markov chain Monte Carlo (MCMC) algorithms for model fitting and Bayesian posterior inference; Section 5 provides the results of a simulation study to assess and compare the proposed model to current methods as well as results from the analysis on two real datasets; Section 6 concludes the article with a summary and discussion of the proposed Bayesian-SBM-MRF model.

2 Data Preparation

In this section, we describe the two sources of binary taxonomic information to perform microbiome community detection; namely, the microbiome co-occurrence network and taxonomic tree, as illustrated in Figure 1.

Let $\mathbf{Y} = [y_{ij}] \in \mathbb{N}^{n \times p}$ denote an $n \times p$ taxonomic abundance matrix, with y_{ij} indicating the count of taxon j observed from sample i , $i = 1, \dots, n, j = 1, \dots, p$. We use $\mathbf{y}_i = (y_{i1}, \dots, y_{ip})^\top$ and $\mathbf{y}_{\cdot j} = (y_{1j}, \dots, y_{nj})^\top$ to denote the vector from the i^{th} row and j^{th} column of \mathbf{Y} , respectively. We use the same formatting for any matrix throughout this paper.

2.1 Microbiome co-occurrence network

Let $\mathbf{X} = [x_{ij}] \in [0, 1]^{n \times p}$ denote the $n \times p$ matrix of the relative abundances (i.e., compositions), where $x_{ij} = y_{ij} / \sum_{j=1}^p y_{ij}$. The vector of relative abundances in the i^{th} sample, \mathbf{x}_i , is defined on a p -dimensional simplex (i.e., $x_{ij} \geq 0, \forall j$ and $\sum_{j=1}^p x_{ij} = 1$). To map a composition to a Euclidean vector space, Aitchison [5] proposed the CLR transformation, which is to scale the relative abundances \mathbf{x}_i by its geometric mean and then take the logarithm to remove the unit-sum constraint. However, taxonomic abundance data contain a large proportion of zero counts attributed to rare or low-abundance taxa that may be present in only a small percentage of samples; whereas, others are not recorded due to the limitations of the sampling effort. The CLR transformation adds an arbitrary pseudo value to both non-zero and zero values, which disguises the zeros and may lead to spurious correlations between taxa because zeros and non-zeros are treated equally. To remedy this issue, Yoon et al. [94] recently proposed MCLR, which transforms only the non-zero values, and they demonstrated that MCLR reduces bias and variance compared to CLR. Specifically, the MCLR transformation, given by Equation (1), takes the log of the ratio of each $x_{ij} \neq 0$ and the geometric mean of all non-zeros in \mathbf{x}_i . Let $\mathbf{V} = [v_{ij}] \in \mathbb{R}^{n \times p}$ denote the $n \times p$ matrix of the MCLR-transformed relative abundances, each element of which is expressed as

$$v_{ij} = \begin{cases} 0 & \text{if } x_{ij} = 0 \\ \log(x_{ij}/\tilde{g}(\mathbf{x}_i)) + \epsilon_i & \text{if } x_{ij} \neq 0 \end{cases}, \quad (1)$$

where $\tilde{g}(\mathbf{x}_i) = \left(\prod_{j=1}^p x_{ij}^{I(x_{ij} \neq 0)} \right)^{\frac{1}{\sum_{j=1}^p I(x_{ij} \neq 0)}}$ gives the geometric mean of the non-zero relative abundances in sample i , where $I(\cdot)$ is the indicator function. MCLR reduces to robust CLR [64] when $\epsilon_i = 0, \forall i$. Alternatively, we can make all non-zero entries strictly positive by letting $\epsilon_i = 1 + \min_{\{j: x_{ij} \neq 0\}} \{|\log(x_{i1}/\tilde{g}(\mathbf{x}_i)), \dots, \log(x_{ip}/\tilde{g}(\mathbf{x}_i))|\}$ as suggested by Yoon et al. [94], which imposes a shift above zero on the transformed values.

While the log transformation is a feature of MCLR, it does not guarantee linearization [69], especially since the transformation only applies to each $x_{ij} \neq 0$. The data remain positively skewed after transformation due to the non-transformed zeros. As a result, to measure the similarity between any pair of taxa j and j' in terms of MCLR-transformed relative abundances (i.e., between $\mathbf{v}_{\cdot j}$ and $\mathbf{v}_{\cdot j'}$), we use their Spearman correlation coefficient $\rho_{jj'}$ to account for non-linearity [23]. We further test the null hypothesis $\rho_{jj'} = 0$ versus the alternative $\rho_{jj'} \neq 0$ and obtain a p -value to determine the significance. All p -values are further adjusted using the Benjamini-Hochberg procedure to control the false discovery rate [11]. To construct the microbiome co-occurrence network represented by a $p \times p$ binary adjacency matrix $\mathbf{G} = [g_{jj'}] \in \{0, 1\}^{p \times p}$, we assigned an edge as $g_{jj'} = 1$ if the corresponding adjusted p -value of $\rho_{jj'}$ is less than the significance level of $\alpha = 0.05$ and zero otherwise.

2.2 Taxonomic tree

We make use of taxonomic tree information by indicating if two taxa (e.g., species) have the same parent (e.g., genus). A tree is an undirected graph where any two nodes are connected by exactly one path. Thus, we describe the taxonomic tree using an adjacency matrix. Let $\mathbf{Q} = [q_{jj'}] \in \{0, 1\}^{p \times p}$ denote a $p \times p$ binary adjacency matrix where $q_{jj'} = 1$ indicates that taxa j and j' have the same parent and zero otherwise for $j \neq j'$. The information from \mathbf{Q} allows the model to include the taxonomic tree information, which is an attractive feature as well as one of the novelties of our model. As a caution, we recommend incorporating only genus or family level at most as parents. If you incorporate information too far up the taxonomic tree, then all the taxa will naturally collapse into one group, rendering useless results. While both \mathbf{G} and \mathbf{Q} are binary adjacency matrices, experts agree that very little information is lost when sequence data are converted to the binary level [87]. For example, binary data have been used for the analysis of gene expression data and have produced reasonable results [87, 33].

3 Model

In this section, we first review the standard Bayesian SBM model in Section 3.1 and then provide the full details about our proposed Bayesian-SBM-MRF in Section 3.2.

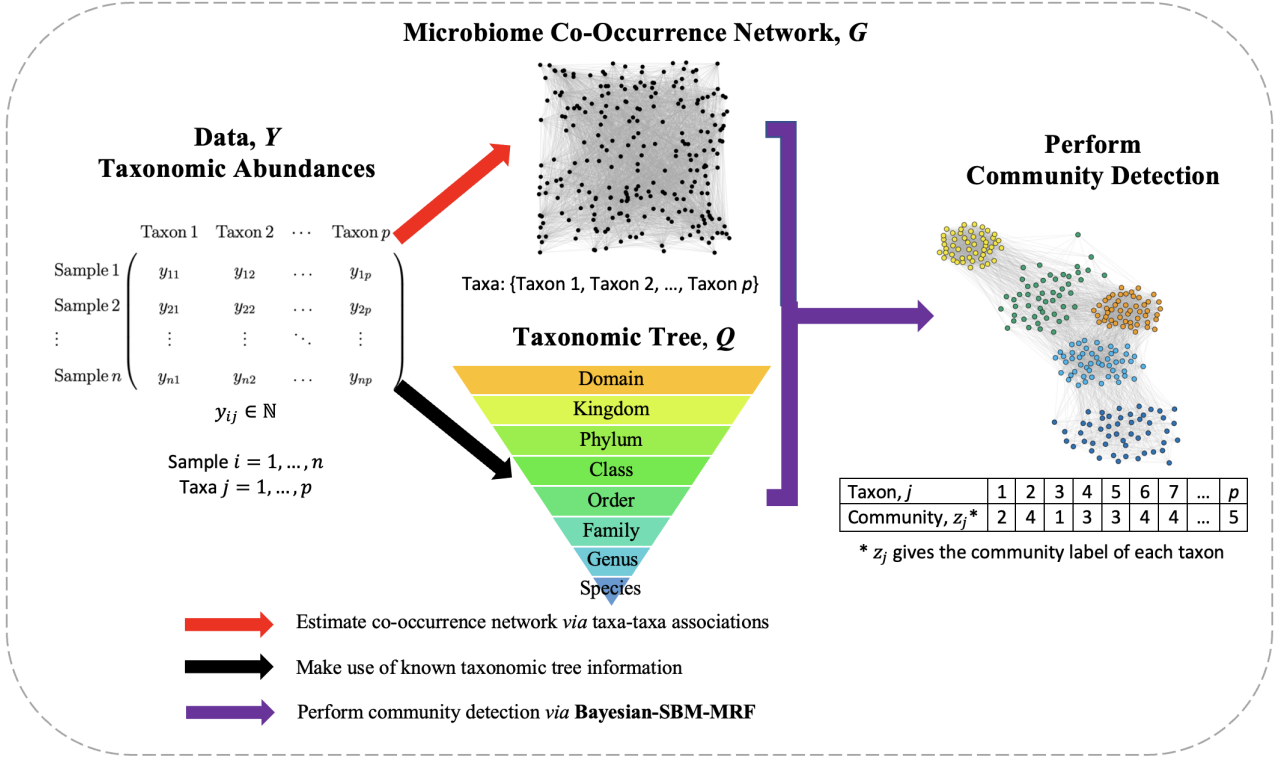


Figure 1: An illustration of Bayesian-SBM-MRF workflow. First, the microbiome co-occurrence network G is estimated from the taxonomic abundance data with n samples and p taxa using a pairwise similarity metric (red arrow). The taxonomic tree Q paired with the taxonomic abundance data is extracted (black arrow). Second, community detection is performed using Bayesian-SBM-MRF to infer the underlying microbiome community structure, indicated by z , by integrating G and Q (purple arrow).

3.1 A Review of the Bayesian Stochastic Block Model

The standard Bayesian SBM for a binary network [66, 71] performs community detection on p taxa to cluster them into K homogeneous communities *via* a finite Bernoulli mixture model that depends on the community indicator vector z and the edge probability matrix Ω , which are independent parameters by assumption. Note that the number of communities is assumed to be fixed and cannot exceed n . Let $z = [z_j] \in \{1, \dots, K\}^{p \times 1}$ denote the community labels for taxon $1, \dots, p$, where $z_j = k$ indicates that taxon j belongs to community k . The total number of taxa belonging to community k is denoted by $n_k = \sum_{j=1}^p I(z_j = k)$. Next, $\Omega = [\omega_{kk'}] \in [0, 1]^{K \times K}$ contains the edge probabilities, where each diagonal element ω_{kk} and each off-diagonal element $\omega_{kk'}, k \neq k'$ indicate the probability of observing an edge between any two taxa within community k and between communities k and k' , respectively.

We assume that the presence of an edge between taxa j and j' in the microbiome co-occurrence network is a Bernoulli random variable conditional on their community memberships,

$$g_{jj'} | z_j = k, z_{j'} = k', \omega_{kk'} \sim \text{Bern}(\omega_{kk'}). \quad (2)$$

Thus, we can express the full data-likelihood as

$$\begin{aligned} f(G|z, \Omega) &= \prod_{k=1}^K \prod_{\{j < j' : z_j = k, z_{j'} = k\}} \text{Bern}(g_{jj'} | \omega_{kk}) \prod_{k < k'} \prod_{\{j < j' : z_j = k, z_{j'} = k'\}} \text{Bern}(g_{jj'} | \omega_{kk'}) \\ &= \prod_{k=1}^K \omega_{kk}^{M_{kk}} (1 - \omega_{kk})^{N_{kk} - M_{kk}} \prod_{k < k'} \omega_{kk'}^{M_{kk'}} (1 - \omega_{kk'})^{N_{kk'} - M_{kk'}}, \end{aligned} \quad (3)$$

where $M_{kk'}$ and $N_{kk'}$ are the number of observed and total possible edges, respectively, within community k or between communities k and k' . Specifically,

$$N_{kk'} = \begin{cases} \binom{n_k}{2} & \text{if } k = k' \\ n_k n_{k'} & \text{if } k \neq k' \end{cases} \quad \text{and } M_{kk'} = \sum_{j=1}^p I(g_{jj'} = 1) I(z_j = k) I(z_{j'} = k'). \quad (4)$$

We model the latent community membership for each taxon, z_j , from a multinomial distribution, which is expressed as

$$z_j | \boldsymbol{\pi} \sim \text{Mult}(1, \boldsymbol{\pi}), \quad (5)$$

where $\boldsymbol{\pi} = (\pi_1, \dots, \pi_K)^\top$ with π_k indicating the size of community k *a priori*. Next, $\boldsymbol{\pi}$ is assumed to be a random variable. So, we place a Dirichlet (Dir) prior on $\boldsymbol{\pi}$, i.e., $\boldsymbol{\pi} \sim \text{Dir}(\boldsymbol{\alpha})$, where $\boldsymbol{\alpha} = (\alpha_1, \dots, \alpha_K)^\top$ is a positive real-valued vector. Without any specific reason, each α_k is usually set to 1 to obtain a uniform hyperprior [38]. Thus, the full conditional posterior density for z_j belonging to community k given everything else can be expressed as

$$\begin{aligned} \pi(z_j = k | \mathbf{z}_{-j}, \boldsymbol{\Omega}, \mathbf{G}) &\propto f(\mathbf{G} | \mathbf{z}, \boldsymbol{\Omega}) \pi(z_j = k, \mathbf{z}_{-j} | \boldsymbol{\pi}) \pi(\boldsymbol{\pi}) \\ &= \prod_{k=1}^K \omega_{kk}^{M_{kk}} (1 - \omega_{kk})^{N_{kk} - M_{kk}} \prod_{k < k'} \omega_{kk'}^{M_{kk'}} (1 - \omega_{kk'})^{N_{kk'} - M_{kk'}} \\ &\quad \times \prod_{k=1}^K \frac{n!}{n_1! \cdots n_K!} \pi_k^{n_k}, \end{aligned} \quad (6)$$

where \mathbf{z}_{-j} denotes all the elements in \mathbf{z} excluding the j^{th} element. Let $\boldsymbol{\eta} = (\eta_1, \dots, \eta_K)^\top$ denote the normalized posterior probability vector for community membership, where $\eta_k = \pi(z_j = k | \mathbf{z}_{-j}, \boldsymbol{\Omega}, \mathbf{G}) / \sum_{m=1}^K \pi(z_j = m | \mathbf{z}_{-j}, \boldsymbol{\Omega}, \mathbf{G})$. Then, we can sample each community membership label, z_j , from a multinomial distribution

$$z_j | \mathbf{z}_{-j}, \boldsymbol{\Omega}, \mathbf{G} \sim \text{Mult}(1, \boldsymbol{\eta}). \quad (7)$$

To complete the model specification, we impose a beta prior on each $\omega_{kk'}$, i.e., $\omega_{kk'} \sim \text{Beta}(a_\omega, b_\omega)$, where a_ω and b_ω are fixed hyperparameters. A common non-informative setting is $a_\omega = b_\omega = 1$ [38]. This conjugate setting results in a beta distribution for the posterior distribution, $\omega_{kk'} | \mathbf{z}, \mathbf{G} \sim \text{Beta}(M_{kk'} + a_\omega, N_{kk'} - M_{kk'} + b_\omega)$.

3.2 Generalized Bayesian Stochastic Block Model with a Markov Random Field Prior

Here, we propose Bayesian-SBM-MRF: the generalized version of the standard Bayesian SBM model from Section 3.1. Bayesian-SBM-MRF integrate two different types of taxonomic information, \mathbf{G} and \mathbf{Q} , illustrated in Figure 1. We propose to replace the multinomial prior shown in Equation (5) with an MRF prior, which can incorporate information from the given taxonomic tree on microbiome community detection. The MRF [12] is a class of parametric models used for spatial data analysis that originated in theoretical physics [20, 19]. Essentially, the MRF is a nearest neighbor problem where we are interested in calculating the conditional probability that a particular taxon j belongs to community k (i.e., $z_j = k$) given all neighboring taxa. In this paper, a neighbor is defined as any two taxa that have the same parent such as genus. Thus, the MRF prior offers a way to incorporate the taxonomic tree information \mathbf{Q} by encouraging two taxa with the same parent to be clustered in the same community. In particular, we write the conditional probability density for z_j belonging to community k given all other taxa memberships \mathbf{z}_{-j} as

$$\begin{aligned} z_j | \mathbf{z}_{-j}, \mathbf{Q} &\sim \text{MRF}(e_k, f), \\ \pi(z_j = k | \mathbf{z}_{-j}, \mathbf{Q}) &\propto \exp \left(e_k + f \sum_{\{j': q_{jj'}=1\}} I(z_{j'} = k) \right), \end{aligned} \quad (8)$$

where $f \in \mathbb{R}_{\geq 0}$ and $e_k = \log(\eta_k)$. The MRF prior in Equation (8) reduces to the prior in Equation (5) when $f = 0$, which means that the standard Bayesian SBM in Section 3.1 is a special case of the proposed generalized model. Additionally, the prior reduces to a non-informative discrete uniform prior when $f = 0$ and $e_k = \log(\eta_k) = \log(1/K)$. For that reason, we set $e_k = \log(1/K)$ in our model. When $f > 0$, the available taxonomic tree information is incorporated into the model from \mathbf{Q} . When f is too large, then $\pi(z_j = k | \mathbf{z}_{-j}) \rightarrow \infty$ and the model undergoes phase transition. A phase transition in a statistical model is concerned with how a small change in a model hyperparameter (e.g., f) can change the state or quality of overall model performance. In our simulation in Section 5.1, we determined that $f = 1$ is a reasonable value for the MRF prior setting.

Then, the full conditional posterior density for the community labels from Equation (6) is updated as

$$\begin{aligned} \pi(z_j = k | \mathbf{z}_{-j}, \boldsymbol{\Omega}, \mathbf{G}, \mathbf{Q}) &\propto f(\mathbf{G} | \mathbf{z}, \boldsymbol{\Omega}) \pi(z_j = k | \mathbf{z}_{-j}, \mathbf{Q}) \\ &\propto \prod_{k=1}^K \omega_{kk}^{M_{kk}} (1 - \omega_{kk})^{N_{kk} - M_{kk}} \prod_{k < k'} \omega_{kk'}^{M_{kk'}} (1 - \omega_{kk'})^{N_{kk'} - M_{kk'}} \\ &\quad \times \exp \left(f \sum_{\{j': q_{jj'}=1\}} I(z_{j'} = k) \right) \end{aligned} \quad (9)$$

Let $\boldsymbol{\xi} = (\xi_1, \dots, \xi_K)^\top$ denote the normalized posterior probability vector for community membership, where $\xi_k = \pi(z_j = k | \mathbf{z}_{-j}, \boldsymbol{\Omega}, \mathbf{G}, \mathbf{Q}) / \sum_{m=1}^K \pi(z_j = m | \mathbf{z}_{-j}, \boldsymbol{\Omega}, \mathbf{G}, \mathbf{Q})$. Then, we can sample each community membership label, z_j , from a multinomial distribution

$$z_j | \mathbf{z}_{-j}, \boldsymbol{\Omega}, \mathbf{G}, \mathbf{Q} \sim \text{Mult}(1, \boldsymbol{\xi}). \quad (10)$$

We follow the standard Bayesian SBM to update the edge probabilities, $\omega_{kk'} | \mathbf{z}, \mathbf{G} \sim \text{Beta}(M_{kk'} + a_\omega, N_{kk'} - M_{kk'} + b_\omega)$, because they are conditionally independent of the community label \mathbf{z} and irrelevant to the taxonomic tree \mathbf{Q} .

4 Model Fitting

In Section 4.1, we first describe the details of the MCMC algorithms based on a two-step Gibbs sampler [31]. Then, we give the details of posterior inference for the parameters of main interest, $\boldsymbol{\Omega}$ and \mathbf{z} , as well as how to select the number of communities K in Section 4.2.

4.1 MCMC Algorithms

Posterior sampling can be easily implemented for Bayesian-SBM-MRF using a two-step Gibbs sampler since both \mathbf{z} and $\boldsymbol{\Omega}$ can be sampled from multinomial and beta distributions, respectively. The Gibbs sampler will be run for T iterations where we discard the first half of posterior samples as burn-in samples. The number of burn-in samples is $B = T/2$ for iterations $t = 1, \dots, B$. Then, the total number of after burn-in posterior samples is $T - B$ for iterations $t = B + 1, \dots, T$. Algorithm 1 illustrates the model fitting steps for Bayesian-SBM-MRF where parameters \mathbf{z} and $\boldsymbol{\Omega}$ are jointly inferred using a Gibbs sampler.

```

Data:  $\mathbf{G}, \mathbf{Q}$ ; fix  $a_\omega, b_\omega, K, T, f$ 
Initialize:  $\mathbf{z}$ 
for  $t$  in  $1 : T$  do
  for  $k$  in  $1 : K$  do
    if  $k \leq k'$  then
       $\omega_{kk'}^{(t+1)} | \mathbf{z}^{(t)}, \mathbf{G} \sim \text{Beta}(a_\omega + M_{kk'}^{(t)}, b_\omega + N_{kk'}^{(t)} - M_{kk'}^{(t)});$ 
    end
  end
  for  $j$  in  $1 : p$  do
    for  $k$  in  $1 : K$  do
       $\xi_k = \pi(z_j^{(t+1)} = k | \mathbf{z}_{-j}^{(t+1)}, \boldsymbol{\Omega}, \mathbf{G}, \mathbf{Q}) / \sum_{m=1}^K \pi(z_j^{(t+1)} = m | \mathbf{z}_{-j}^{(t+1)}, \boldsymbol{\Omega}, \mathbf{G}, \mathbf{Q})$ 
    end
     $z_j^{(t+1)} | \mathbf{z}_{-j}^{(t+1)}, \boldsymbol{\Omega}, \mathbf{G}, \mathbf{Q} \sim \text{Mult}(1; \boldsymbol{\xi});$ 
  end
  Store:  $\boldsymbol{\Omega}^{(t+1)}, \mathbf{z}^{(t+1)}$ ;
end

```

Algorithm 1: Gibbs Sampler for Bayesian-SBM-MRF

4.2 Posterior Inference

We make three inferences that will provide a comprehensive scope of the community structure of the microbiome co-occurrence network from the resulting posterior samples. The first is to infer the edge probabilities in $\boldsymbol{\Omega}$ so that we can assess the relationship of all taxa within and between the communities. The second is to identify

the community labels of all the taxa given by the parameter \mathbf{z} . Thirdly, we would like to infer the optimal value of K to estimate the appropriate number of communities.

Bayesian inference commonly uses simple numerical summaries such as the posterior mean to obtain a point estimate of a model parameter [38]. The point estimate for each $\omega_{kk'} \in \Omega$ is computed as the posterior mean of the after burn-in posterior samples, which is given by

$$\hat{\omega}_{kk'} = \frac{1}{T - B} \sum_{t=B+1}^T \omega_{kk'}^{(t)} \quad (11)$$

where t is the current iteration of the MCMC algorithm after a burn-in period.

Next, we infer the community labels of all p taxa *via* the parameter \mathbf{z} . We could identify the $\mathbf{z}^{(t)}$ at a particular iteration t (after burn-in) that maximizes the posterior distribution. This is known as the *maximum a posteriori* (MAP) estimate and is denoted as $\hat{\mathbf{z}}^{\text{MAP}}$. Specifically,

$$\hat{\mathbf{z}}^{\text{MAP}} = \arg \max_{\mathbf{z} \in \{\mathbf{z}^{(B+1)}, \dots, \mathbf{z}^{(T)}\}} \pi(\mathbf{z}, \Omega | \mathbf{G}, \mathbf{Q}). \quad (12)$$

Bayesian information criterion (BIC) [80] is one popular metric for determining the optimal number of communities for model-based clustering algorithms [84, 67]. BIC is defined as

$$\text{BIC} = \nu \log p - 2 \left(\arg \max_{\pi(\mathbf{z}, \Omega | \mathbf{G}, \mathbf{Q})} \log \pi(\mathbf{z}, \Omega | \mathbf{G}, \mathbf{Q}) \right) \quad (13)$$

where ν is the number of model parameters and p is the number of taxa. The number of parameters is $\nu = 1 + K(K + 1)/2$ since we have to estimate \mathbf{z} and $K(K + 1)/2$ edge probabilities given by each $\omega_{kk'} \in \Omega$. BIC is an appropriate metric when the sample size n is greater than the number of model parameters [34], which was not an issue for all analyses in Section 5.

5 Results

In this section, we describe the generative model in our simulation study and demonstrate the superior performance of Bayesian-SBM-MRF through both simulation and two case studies of very different kinds.

5.1 Simulation

We constructed co-occurrence networks with species-level taxa as nodes that are grouped into K communities. In particular, we sampled each edge of the network as $g_{jj'} | \omega_{kk'} \sim \text{Bernoulli}(\omega_{kk'})$. To incorporate the taxonomic tree information, we randomly assigned each of the p species to a community and genus using three strength settings (weak, moderate, and strong). Strength here describes how informative the taxonomic tree information can be for community detection. Let $\boldsymbol{\tau} = (\tau_1, \dots, \tau_p)^\top$ specify the genus labels for species $1, \dots, p$. We used the adjusted Rand index (ARI) [77], which is a similarity metric between two sets of discrete labels (e.g., community and genus), to classify strength. Equation (14) below shows how to compute ARI, which usually takes on values between 0 and 1. An ARI close to zero indicates little to no similarity between community and genus, and closer to one indicates strong similarity. We considered the tree information to be weakly informative if the ARI between the genus and community labels was low (e.g., $\text{ARI}(\mathbf{z}, \boldsymbol{\tau}) \leq 0.3$). Next, the tree information was moderately informative if $0.3 < \text{ARI}(\mathbf{z}, \boldsymbol{\tau}) \leq 0.7$ and strongly informative if $0.7 < \text{ARI}(\mathbf{z}, \boldsymbol{\tau}) \leq 1$. Table 1 gives examples of the weak, moderate, and strong settings for ten taxa ($j = 1, \dots, 10$) and two communities ($z_j \in \{1, 2\}$). Each genus τ_j is a natural number. Under the weak setting where $\text{ARI}(\mathbf{z}, \boldsymbol{\tau}) = 0$, none of the taxa belong to the same genus, and so there is no similarity between community and genus. The moderate setting where $\text{ARI}(\mathbf{z}, \boldsymbol{\tau}) = 0.5$ illustrates a fair level of similarity between the genus and community where the taxa from the first community all belong to the same genus; however, the taxa in the second community all belong to distinct genera. The strong setting where $\text{ARI}(\mathbf{z}, \boldsymbol{\tau}) = 1$ illustrates the perfect scenario where taxa belonging to the first community all belong to the same genus and taxa in the second community all belong to another genus. Additionally, diversity can be inferred from the strength of the taxonomic tree information. As the level of strength weakens, the diversity in genus increases. Similarly, diversity decreases and strength increases.

Next, we simulated co-occurrence networks that are composed of $K = \{3, 6, 9\}$ communities and $p = 180$ species-level taxa. Edge probabilities between communities are typically low, so we randomly sampled these edges from a uniform distribution such that $\omega_{kk'} \sim \text{Uniform}(0, 0.1)$ for $k \neq k'$. The probability of an edge between two taxa within the same community $\omega_{kk'}$ where $k = k'$ took on preset values between 0 and 1 to imitate various levels of taxon-taxon interaction in each community. Specifically, $\omega_{kk'} = \{0.3, 0.6, 0.95\}$ for $k = 1, \dots, 3$ (i.e., $K = 3$), $\omega_{kk'} = \{0.1, 0.3, 0.5, 0.7, 0.9, 0.97\}$ for $k = 1, \dots, 6$ (i.e., $K = 6$), and $\omega_{kk'} =$

Table 1: Examples of weak, moderate, and strong simulation settings with $p = 10$ taxa and $K = 2$ communities. τ_j and z_j give the genus and community of taxa j , respectively, for $j = 1, \dots, 10$. The quantity $\text{ARI}(\boldsymbol{\tau}, \boldsymbol{z})$ gives the ARI between genus and community.

	Taxon j									
	1	2	3	4	5	6	7	8	9	10
	Weak Setting									
τ_j (Genus)	15	10	17	6	11	9	25	29	3	1
z_j (Community)	1	1	1	1	1	2	2	2	2	2
	$\text{ARI}(\boldsymbol{\tau}, \boldsymbol{z}) = 0$									
	Moderate Setting									
τ_j (Genus)	15	15	15	15	15	3	4	26	7	8
z_j (Community)	1	1	1	1	1	2	2	2	2	2
	$\text{ARI}(\boldsymbol{\tau}, \boldsymbol{z}) \approx 0.5$									
	Strong Setting									
τ_j (Genus)	15	15	15	15	15	8	8	8	8	8
z_j (Community)	1	1	1	1	1	2	2	2	2	2
	$\text{ARI}(\boldsymbol{\tau}, \boldsymbol{z}) = 1$									

$\{0.12, 0.2, 0.3, 0.4, 0.5, 0.7, 0.8, 0.9, 0.99\}$ for $k = 1, \dots, 9$ (i.e., $K = 9$). We included 30 genera in total where $\tau_j \in \{1, \dots, 30\}$ for each taxon $j = 1, \dots, 180$. Altogether, there were $3 \times 3 = 9$ settings in this simulation. For each scenario, we repeated the above steps to generate 50 replicates.

First, we wanted to determine if Bayes-SBM-MRF improves the performance of the standard Bayesian SBM by incorporating taxonomic tree information. We compared the results of Bayesian-SBM-MRF under four settings of the MRF prior when $f = \{0, 0.5, 1, 2\}$. When $f = 0$, the standard Bayesian SBM is employed since no taxonomic tree information is incorporated. This setting was then compared to the other three when $f > 0$ where Bayes-SBM-MRF incorporates taxonomic tree information. Second, we compared these four settings to two commonly used competing clustering models selected from Table 3: the `cluster_fast_greedy` function from the very popular `igraph` package in R, and spectral clustering from the `anocva` package in R.

We assessed the performance of all models on the 50 replicated data sets under each setting to determine how well they can recover the true community labels \boldsymbol{z} . One popular similarity metric for comparing the predicted and true community labels to assess model quality is ARI, which is useful for dealing with the issue of community label switching that is common to clustering algorithms [43]. ARI is a corrected version of the Rand index so that label switching is not an issue when comparing predicted and true community labels. For example, an algorithm may estimate the community labels of four taxa to be $\hat{\boldsymbol{z}} = \{1, 1, 2, 2\}$ while the underlying truth may be $\boldsymbol{z} = \{2, 2, 1, 1\}$. Both sets of labels are equivalent because the first two taxa are assigned to the same community and the other two taxa are assigned to the other community. Thus, the community label does not matter since it is a nominal-level variable. ARI is calculated as

$$\text{ARI}(\boldsymbol{z}, \hat{\boldsymbol{z}}) = \frac{\binom{p}{2}(a+d) - [(a+b)(a+c) + (c+d)(b+d)]}{\binom{p}{2}^2 - [(a+b)(a+c) + (c+d)(b+d)]} \quad (14)$$

where $a = \sum_{j>j'} \mathbf{I}(z_j = z_{j'})\mathbf{I}(\hat{z}_j = \hat{z}_{j'})$, $b = \sum_{j>j'} \mathbf{I}(z_j = z_{j'})\mathbf{I}(\hat{z}_j \neq \hat{z}_{j'})$, $c = \sum_{j>j'} \mathbf{I}(z_j \neq z_{j'})\mathbf{I}(\hat{z}_j = \hat{z}_{j'})$ and $d = \sum_{j>j'} \mathbf{I}(z_j \neq z_{j'})\mathbf{I}(\hat{z}_j \neq \hat{z}_{j'})$, respectively. ARI is usually bounded between zero and one, but it may take on small negative values. An ARI closer to one indicates greater similarity between the predicted and true community labels, which provides evidence that the model can recover the underlying communities of a microbiome co-occurrence network.

Results comparing the ARI of the four settings of Bayes-SBM-MRF are displayed in Figure 2. ARI was computed using the `ARI` function from the `aricode` library in R. We performed the paired Mann-Whitney-Wilcoxon test to compare the standard Bayesian SBM when $f = 0$ to the other three settings of our generalized model. Several important observations stand out about our generalized SBM model. The first is that when the level of strength of the taxonomic tree information is moderate or high, Bayes-SBM-MRF where $f > 0$ has significantly higher ARI than the standard Bayesian SBM where $f = 0$. This indicates that the taxonomic tree information can be useful and more powerful for recovering the true community labels, especially when it is informative. Second, there are no significant differences between all four model settings when strength is weak, which indicates that the inclusion of taxonomic tree information does not hurt the performance of our generalized model even when it is not informative. Third, we recommend using $f = 1$ for Bayes-SBM-MRF because it performs equally or better than the other settings. When $K = 9$ and strength is weak, the boxplot corresponding to $f = 2$ is very negatively skewed, indicating the start of a possible phase transition. Next, the boxplots of the ARI for all competing models in Figure 3 demonstrate that Bayesian-SBM-MRF has superior performance under all nine settings. Also, Bayesian-SBM-MRF has consistent ARI as K increases; whereas, the

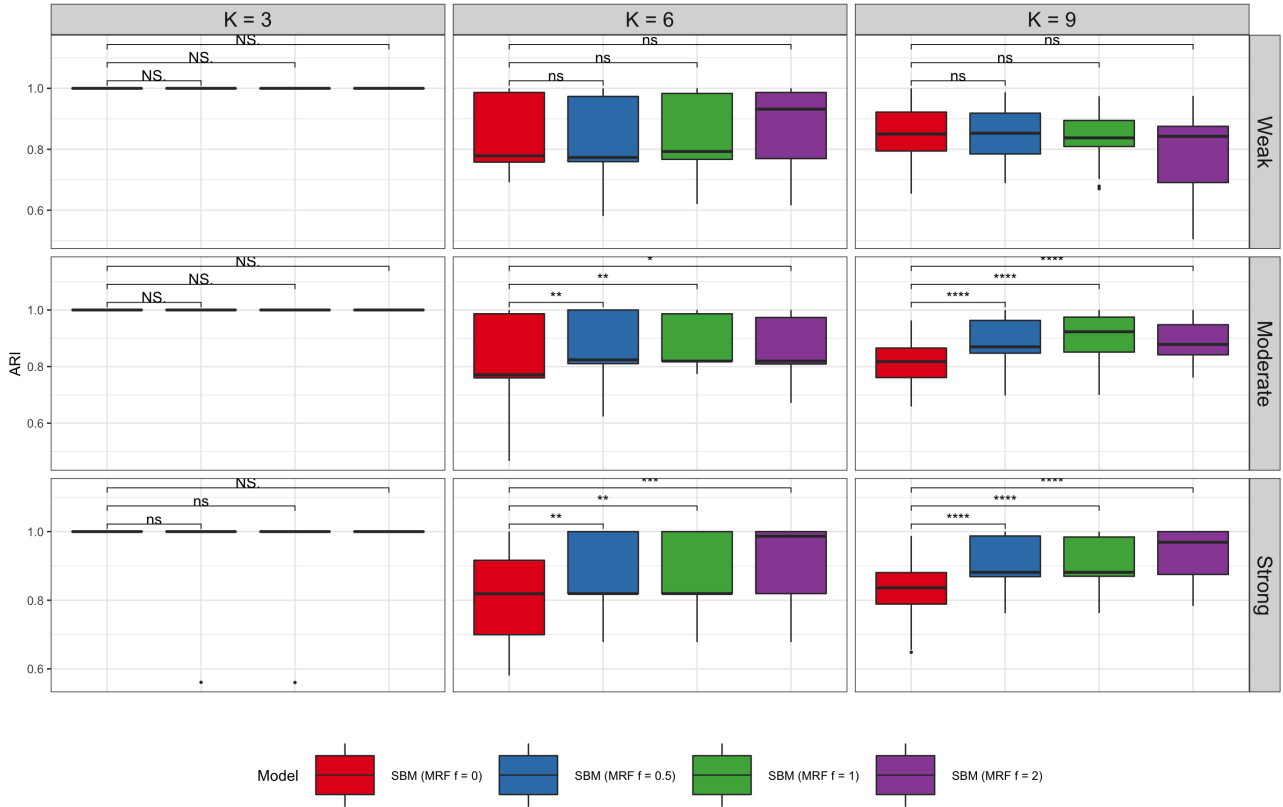


Figure 2: Boxplots of adjusted Rand index (ARI) with four settings of the MRF prior ($f = \{0, 0.5, 1, 2\}$) for the simulated data sets under nine settings of combined number of communities $K = \{3, 6, 9\}$ and the level of informative strength of the taxonomic tree information {Weak, Moderate, Strong}. The paired Mann-Whitney-Wilcoxon test was performed to compare the prior setting where $f = 0$ to the other settings where $f > 0$ to assess model performance with and without taxonomic tree information. Significance is indicated by * ($p < 0.05$), ** ($p < 0.01$), *** ($p < 0.001$), **** ($p < 0.0001$), ns (not significant with $p \in (0.05, 1)$), NS (not significant with $p = 1$).

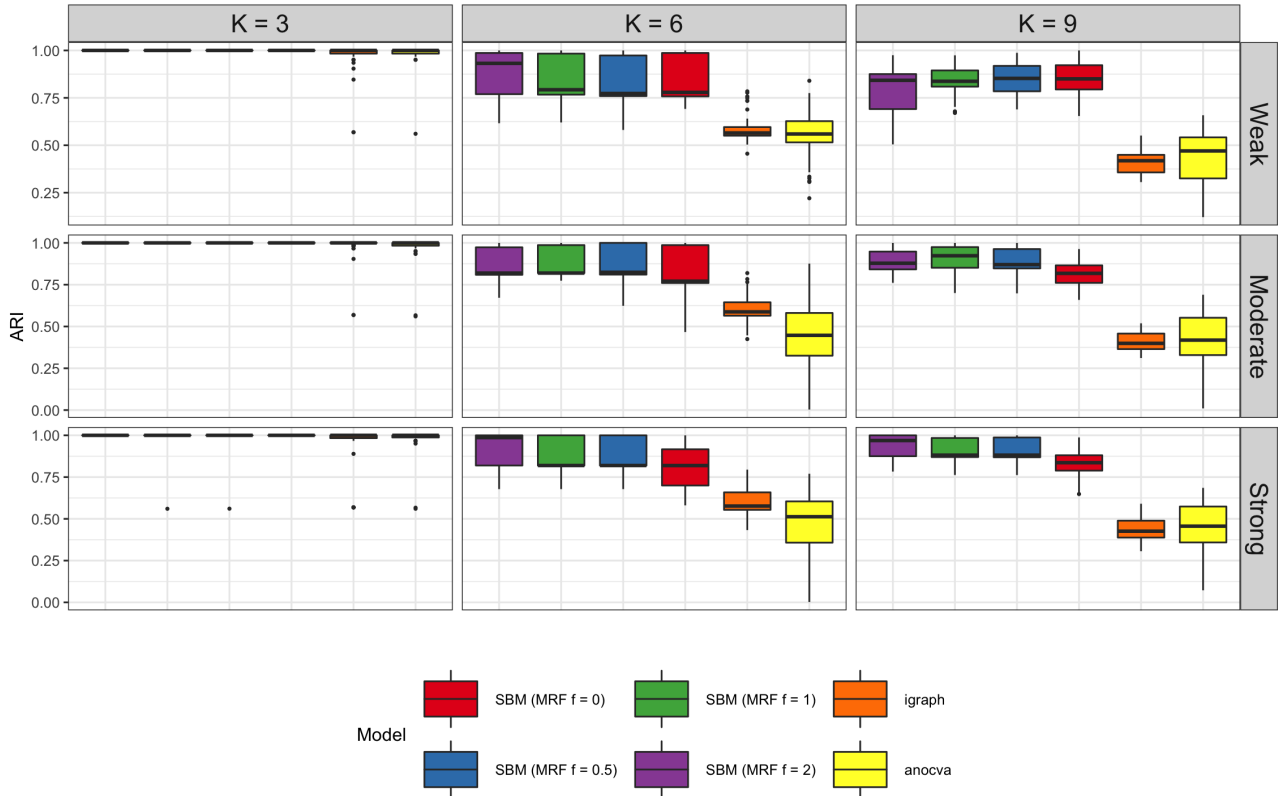


Figure 3: Boxplots of adjusted Rand index (ARI) with four settings of the Markov random field prior ($f = \{0, 0.5, 1, 2\}$) compared to two competing methods: `cluster_fast_greedy` function from the `igraph` library in R, and spectral clustering from the `anocva` library in R. The simulated data sets had nine combined settings of the number of communities $K = \{3, 6, 9\}$ and the level of informative strength of the taxonomic tree information {Weak, Moderate, Strong}.

ARI of the competitors decreases as K increases. This implies that the competing methods are unreliable when there may be many underlying communities. Our method is consistent for both small and large values of K .

5.2 Real Data Analysis 1: Urinary Microbiome Data

We applied Bayesian-SBM-MRF to the urinary microbiome data from our study on rUTI with $n = 75$ postmenopausal female patients. This is the first time anyone has studied the network and community structure of the urinary microbiome with respect to rUTI in postmenopausal women. The urinary microbiome data originally had 180 bacterial species along with their known genera. We filtered out all species that had fewer than seven non-zero counts, which resulted in a total of $p = 99$ species from 41 genera. Of the 41 genera, 18 of these had at least two species belonging to the same genus. About 77% of the bacterial species belong to these 18 genera. Each of the remaining 23% of species belongs to unique genera. The full details regarding the study, data, and metagenomic sequencing can be found in Neugent et al. [68].

The microbiome co-occurrence network \mathbf{G} was estimated from the species-level abundance data and the available taxonomic tree information was incorporated into \mathbf{Q} as described in Section 2. The MCLR transformation was done using the `MCLR` function from the `SPRING` library in R. Then, we performed community detection on \mathbf{G} using Bayesian-SBM-MRF with $f = 1$ for the MRF prior setting. We set $\eta_k = \log(1/K)$ to impose a non-informative discrete uniform prior on each community label $z_j \in \mathbf{z}$. We set $a_\omega = b_\omega = 1$ to impose a non-informative uniform prior on each edge probabilities $\omega_{kk'} \in \Omega$. We ran $T = 1000$ iterations, with the first half of the iterations discarded as burn-in samples.

Our Bayesian-SBM-MRF selected $K = 7$ communities *via* BIC as the optimal number of communities (see the elbow plot in Figure 8 in the appendix). Figure 4 is the heatmap of the estimated microbiome co-occurrence network organized into the seven communities determined by Bayesian-SBM-MRF with $K = 7$. Names of genus and species are in the margins along with their community label number. The main diagonal runs from bottom-left to top-right and represents the seven communities along with the taxa that interact within those communities. These seven communities on the main diagonal are arranged in order from least to greatest

within-community edge probabilities (i.e., darker indicates higher edge probability). The off-diagonal blocks represent between-community interactions. As we can see, communities 6 and 7 at the top right of the main diagonal are equally as dark, indicating that they have about the same edge probability. Even though they are very similar in that sense, the model distinguishes them because their interactions with other communities are very different. The 7th community has high interaction with communities 4 and 5; whereas, community 6 barely interacts with any other community. Even though we imposed a discrete uniform prior on the community labels, notice that the community sizes are quite different. This seems to indicate that there is a good balance of information coming from both the microbiome co-occurrence network and the taxonomic tree information to inform community detection.

We calculated the nodal strength with respect to genus in each community as a way to compare and classify the detected communities. Nodal strength is defined as the sum of all edge weights of a single taxon [36]. Nodal strength for taxon j is denoted as d_j and is computed as

$$d_j = \sum_{j'=1}^p I(g_{jj'} = 1). \quad (15)$$

Since \mathbf{G} is binary, nodal strength is simply nodal degree. Next, we summed each d_j for all taxa in the same community belonging to the same genus to calculate the genus-level nodal strength within each community. This can help to compare both community and network structures. The circular bar plot in Figure 5 displays the genus-level nodal strength (as frequency) in each of the seven communities. The communities and the genera within those communities have evidence-based characteristics that are of biological interest. These characteristics are noted in the plot annotations next to each respective community. For example, communities 3 and 5 are associated with the human skin microbiome [18]. In communities 2, 4, 6, and 7, we also found four distinct microbiome communities harboring taxa known to be markers of dysbiosis in the female urinary microbiome from genera such as *Gardnerella*, *Prevotella*, *Streptococcus*, and *Peptoniphilus* [68, 17, 82].

We also compared the results of standard SBM (i.e., when $f = 0$; genus information is not used) to the results above. Table 2 gives some promising insight into our model’s behavior. When $f = 1$, we found at least six genera that appear in fewer communities than when $f = 0$. While the genera *Peptoniphilus*, *Staphylococcus*, and *Facklamia* collapsed into one community, other genera did not follow the same pattern. *Atopobium* collapsed from three to two communities, *Corynebacterium* collapsed from four to two communities, and *Anaerococcus* collapsed from four to three communities. All other genera showed no changes in the number of assigned communities. Thus, Bayesian-SBM-MRF does not simply force species from the same genus into one community. These observations indicate that Bayesian-SBM-MRF is well-behaved because it is likely making a balanced use of both the microbiome co-occurrence network \mathbf{G} and the taxonomic tree information \mathbf{Q} . The remaining analysis focuses on the difference in diversity of genera per community for $f = 0$ versus $f = 1$.

Table 2: The number of communities that select genus have been assigned to under two different settings ($f = 0$ and $f = 1$) of the generalized model.

Genus	$f = 0$	$f = 1$
<i>Peptoniphilus</i>	2	1
<i>Facklamia</i>	2	1
<i>Bifidobacterium</i>	2	1
<i>Staphylococcus</i>	2	1
<i>Atopobium</i>	3	2
<i>Corynebacterium</i>	4	2
<i>Anaerococcus</i>	4	3

Figure 9 in the appendix illustrates the difference in community structure using both within-community and between-community nodal strength with respect to genus for both the standard Bayesian SBM and Bayesian-SBM-MRF ($f = 0$ and $f = 1$, respectively). The figure suggests that there is some difference in diversity within several communities while a few other communities display little to no difference with respect to genus. To quantify the diversity of genera in each community, we further calculated the Shannon index for both models. The Shannon index is the log transformation of the weighted geometric mean of proportional species per genus in a given community [86]. In general, the Shannon index H is calculated as

$$H = - \sum_{r=1}^R w_r \log(w_r) \quad (16)$$

where R is the number of genera and w_r is the proportion of species belonging to the r^{th} genus in a given community. Figure 6 compares the Shannon indices of the two model settings when $f = 0$ and $f = 1$. The

f = 1

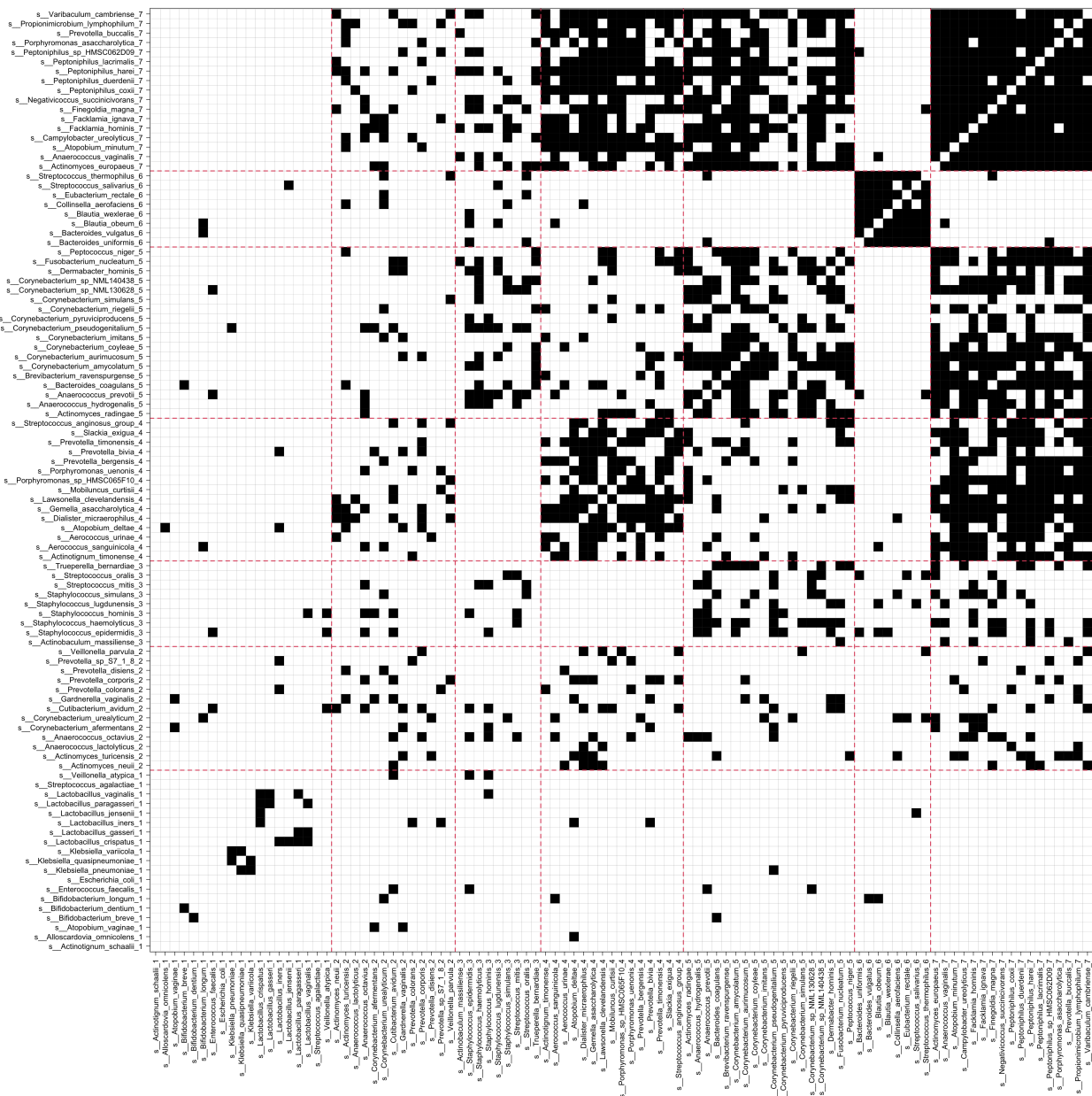


Figure 4: A heatmap of $K = 7$ communities detected by Bayesian-SBM-MRF ($f = 1$). Names of genus and species are in the margins along with their community label number. The main diagonal represents the seven communities determined by the model and their within-community interactions. Off-diagonal blocks represent the between-community interactions. Black indicates a significant association between two taxa and white indicates otherwise.

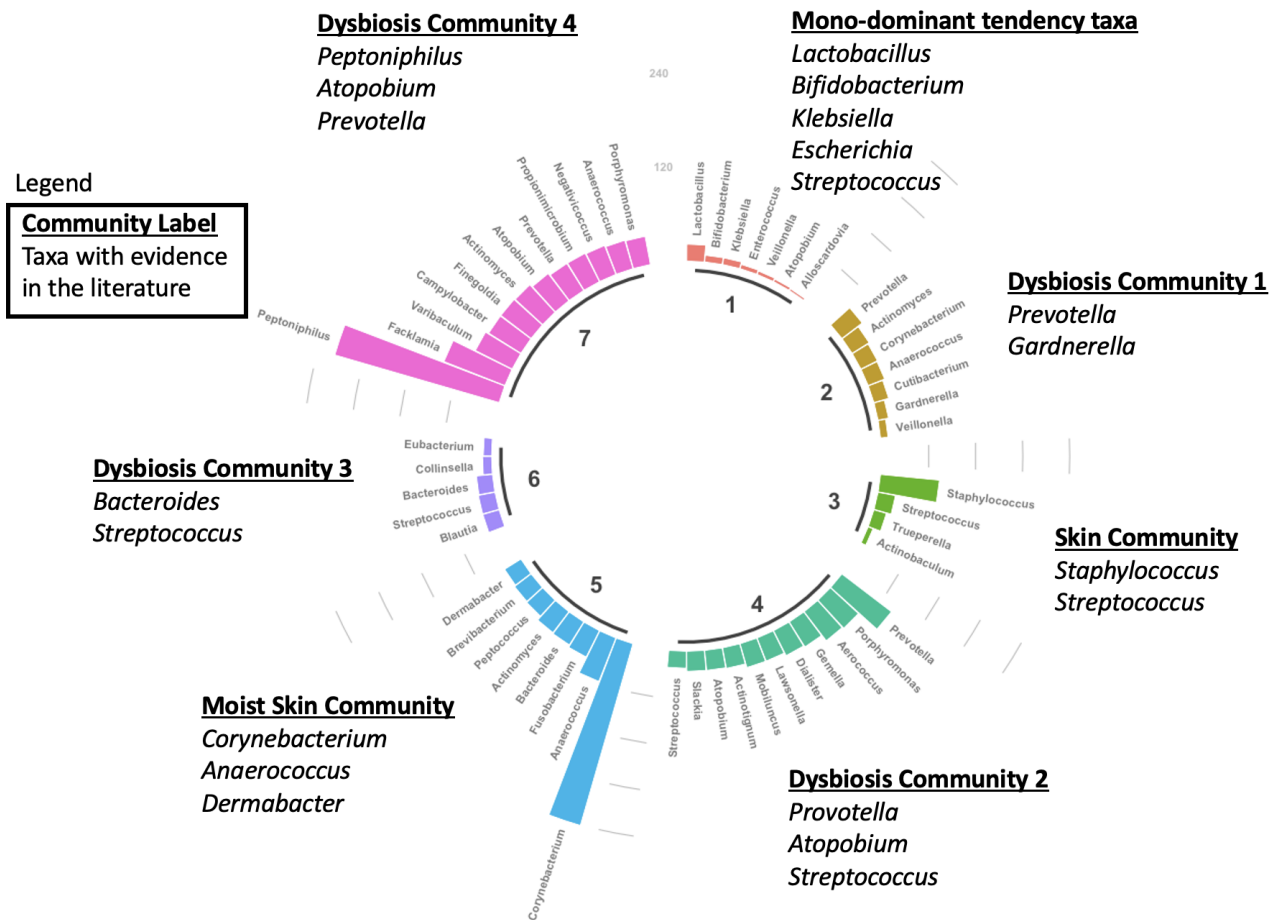


Figure 5: A circular bar plot of $K = 7$ communities detected by Bayesian-SBM-MRF ($f = 1$). Labels on the bars identify the genera found in each community. Bar frequency gives the nodal strength of each genus per community. Annotations identify genera with evidence-based characteristics.

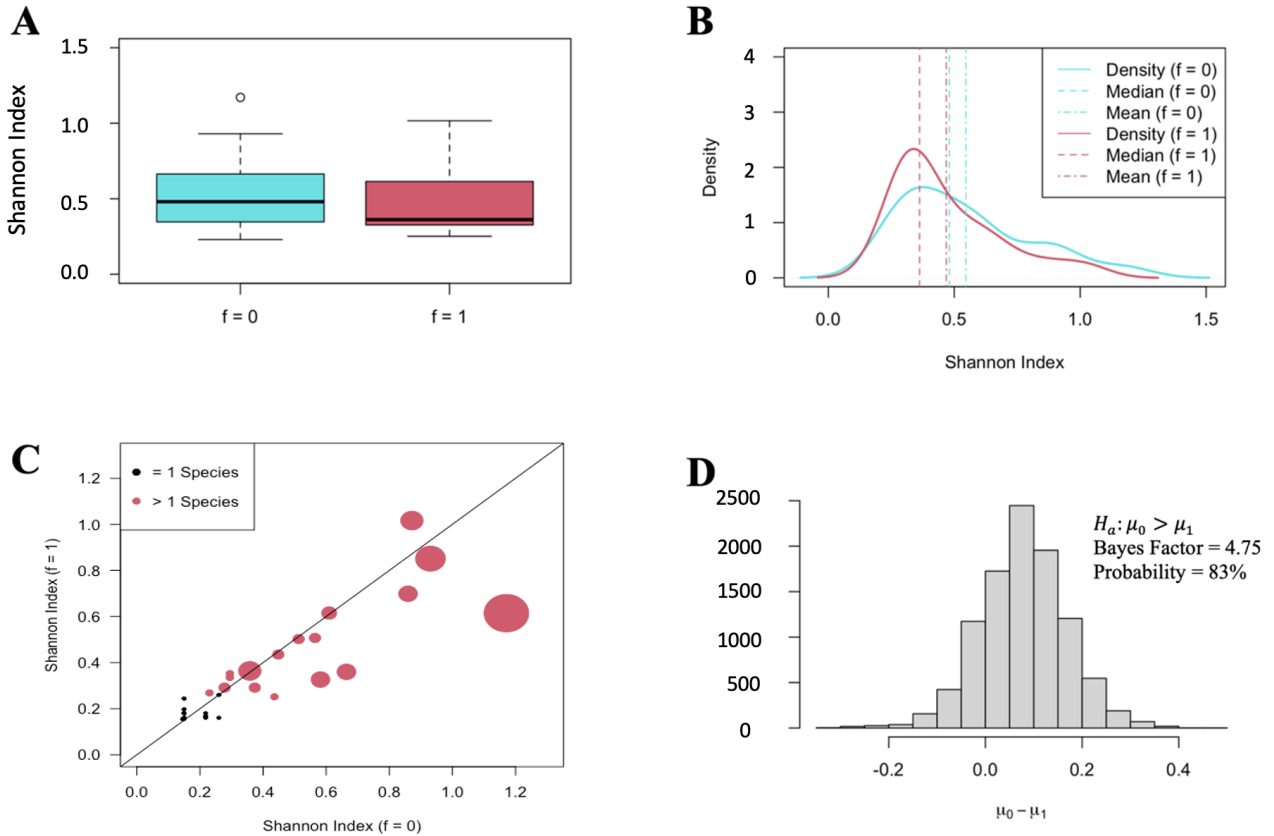


Figure 6: Plots of the Shannon index of the 41 genera pertaining to the standard Bayesian SBM ($f = 0$) and Bayesian-SBM-MRF ($f = 1$). **A**: Boxplots of the Shannon index comparing the diversity of the two models; **B**: Density plots; **C**: Scatter plot of Shannon index of $f = 0$ versus $f = 1$; the size of points varies with respect to the number of species **D**: Histogram of the estimated posterior distribution of the difference in Shannon index means of the two models, Bayes factor and posterior probability in favor of the alternative hypothesis.

boxplots (Figure 6A) compare the median diversity. The density plots (Figure 6B) illustrate the means and medians of the Shannon index distributions for each setting. The scatterplot (Figure 6C) illustrates the diversity of the 41 genera for $f = 1$ versus $f = 0$ where the size and color of each point is based on the number of species per genus (i.e., nodal strength). The points tend to fall below the 45° line indicating lower diversity in the communities when $f = 1$. We used Bayesian hypothesis testing to determine if there is any significant difference between the Shannon index means of the two models. We assumed a normal model with unknown mean and variance. The histogram (Figure 6D) of the difference in the Shannon index means $\mu_0 - \mu_1$ for $f = 0$ versus $f = 1$ is given. The hypotheses of interest are $H_0 : \mu_0 = \mu_1$ versus $H_a : \mu_0 > \mu_1$ since we wish to determine if the mean diversity is significantly lower when $f = 1$. We made inferential decisions based on Bayes Factor and the posterior probability in favor of the alternative hypothesis. According to Jeffreys’ rule [47], a Bayes factor between 3.2 and 10 indicates substantial evidence to reject the null hypothesis. Here, the Bayes factor is 4.75 with 83% posterior probability in favor of the alternative hypothesis over the null hypothesis. The use of taxonomic tree information reduces the diversity in the communities, indicating that the results of the standard Bayesian SBM and our Bayesian-SBM-MRF are substantially different.

5.3 Real Data Analysis 2: *Les Misérables* Data

Co-occurrence networks have been found to be particularly useful in analyzing large text. Here, we demonstrate that our method can be applied to a co-occurrence network derived from a large and structured collection of text.

Les Misérables is a French historical fiction novel written by Victor Hugo in the nineteenth century. The novel is comprised of 1462 pages with 77 characters. The main character, Jean Valjean, is a loner who is on the run most of his life because he broke his parole after being released from a 19-year prison sentence for stealing bread to feed his starving family. The story focuses on his interactions with characters throughout his life, such as Javert (the policeman who spends his life hunting down Valjean for breaking his parole), Myriel (the bishop who gives Valjean shelter for the night; gives Valjean a second chance at freedom after he is caught stealing from the bishop’s home), Fantine (the woman who on her death bed entrusts her young daughter Cosette into

Valjean’s care), Monsieur and Madame Thénardier (the thieving innkeepers who were the caretakers of Cosette until Valjean comes along), Marius (a student of the French Revolution who falls in love with Cosette; an older Valjean saves this young man’s life during the revolution so that he can marry Cosette), and Eponine (who is secretly in love with Marius and is the daughter of the Thénardier’s). The story also includes tertiary characters such as prisoners, prostitutes, students, servants, etc.

The *Les Misérables* data [48] are an undirected graph \mathbf{G} of $p = 77$ nodes. Each node represents a character. An edge is assigned between any two characters if they appear in the same chapter. Edges were also weighted based on the number of co-appearances of any two characters in the same chapter. We utilized the edge weights to construct matrix \mathbf{Q} for the MRF prior. Major characters should have a higher frequency of interaction in any given chapter. Tertiary characters, or minor characters, will have lower frequency. So, we decided that if two characters’ edge weight was greater than two, then $q_{jj'} = 1$ and zero otherwise. Thus, the matrix \mathbf{Q} helps to distinguish tertiary and non-tertiary characters. The network \mathbf{G} cannot distinguish character types because all existing edges are equally weighted since they are binary. We ran Bayesian-SBM-MRF with the same settings as the urinary microbiome data analysis.

The model selected $K = 6$ communities *via* BIC when $f = 1$ (see the elbow plot in Figure 10 in the appendix). Figure 7 illustrates the six communities. This plot was generated in Gephi version 0.10.1 [10]. The size of a node was determined by nodal strength, just as in the previous analysis. The most interesting result is that Valjean is in a community by himself, which makes sense in the context of the story since Valjean is the primary character portrayed as a loner and having brief interactions with most characters. The next community of interest is the blue dots, which includes secondary characters with large roles such as the Thenardier’s, Javert, Eponine, and Cosette. The green community includes the young students and Gavroche who almost all died in the French Revolution. The orange community includes mostly prostitutes and Fantine, the mother of Cosette, who dies early in the story from tuberculosis shortly after having no choice but to become a prostitute herself to support her child. The purple community contains the judge and criminals. Valjean is in prison with these criminals at the beginning of the novel. One of the prisoners, Bamatabois, also interacts with Fantine by viciously demanding her services. Lastly, the yellow dots are tertiary characters (e.g., Child 1, Child 2, Woman 1, Woman 2), who appear very briefly throughout the novel. Lastly, we analyzed these data using the standard Bayesian SBM ($f = 0$) for the sake of comparison. All characters remained in the same communities except for Cosette. Cosette was placed into the community of tertiary characters, which makes no sense since she is a main character. By including additional information *via* the MRF prior, Bayes-SBM-MRF returned a slightly different but more sensible result than the standard Bayesian SBM. This demonstrates that Bayesian-SBM-MRF does a better job at performing community detection than the standard Bayesian SBM and can be broadly applied to other types of network data.

6 Discussion

In this article, we develop a two-stage method for community detection on a microbiome co-occurrence network. The first stage estimates the microbiome co-occurrence network from the MCLR-transformed relative abundances to account for their compositionality, non-linearity, and zero-inflation. We believe this is the first time the MCLR transformation has been used for community detection. The second stage takes the estimated microbiome co-occurrence network and available taxonomic tree information into account to perform community detection using a generalized SBM model, Bayesian-SBM-MRF. We believe that Bayesian-SBM-MRF is the first of its kind to include two levels of the taxonomic tree to perform community detection. The simulation study revealed several advantages of Bayesian-SBM-MRF. First, the inclusion of taxonomic tree information improves model performance when it is informative. Second, the inclusion of taxonomic tree information does not hurt model performance even when it is non-informative. Third, Bayesian-SBM-MRF demonstrated superior performance over commonly used competing methods in all simulation settings. When applied to a real urinary microbiome data set from a study on rUTI from postmenopausal women, Bayesian-SBM-MRF uncovered several communities characterized by evidence-based dysbiosis. Further, this was the first time community detection has been done to study the urinary microbiome co-occurrence network and community structure with respect to rUTI from postmenopausal women. Our findings provide the foundation for future studies in this particular area of research. Additional studies will be required to validate the biological relevance of these communities and their association with rUTI. The application of Bayesian-SBM-MRF to the *Les Misérables* data demonstrates that our model can also be broadly applied to other types of undirected networks. Bayesian-SBM-MRF is more appropriate for microbiome co-occurrence networks because a stochastic model can handle a high-dimensional network; however, it provides reasonable results for other applications and smaller networks.

There are several limitations of Bayesian-SBM-MRF. As mentioned above, our method accounts for zero-inflation in the abundance data using an external normalization step (i.e., the MCLR transformation). Other methods, such as HARMONIES [42] and SPRING [94], proposed zero-inflated model-based methods for estimating a network using probability distributions such as the zero-inflated negative binomial distribution. Both methods

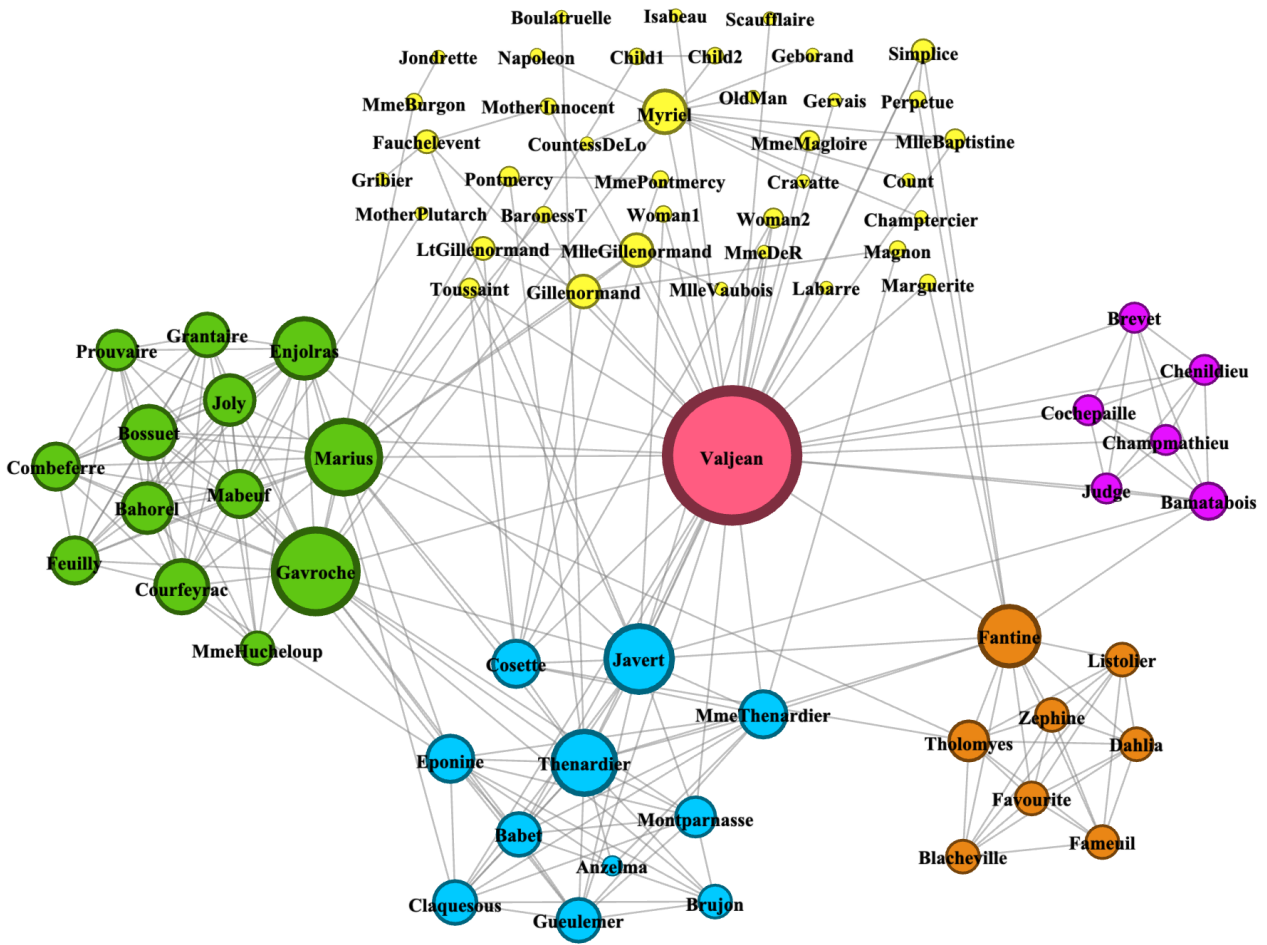


Figure 7: The network of characters from *Les Misérables* and the six communities determined by Bayesian-SBM-MRF. Each color denotes a distinct community. Each edge indicates that two characters appear in the same chapter at least once. Nodal size was determined by nodal strength.

demonstrated superior performance over well-known network analysis methods using model-based or internal normalization. Bayesian-SBM-MRF is a multi-stage model that first estimates the microbiome co-occurrence network and then performs community detection. Previous studies have demonstrated that a joint model is more efficient and may have superior performance when compared to multi-stage models [52, 59, 98, 49, 41]. There are alternative methods in the literature for determining the optimal number of communities. While BIC is standard and widely used, some issues exist. BIC may be unreliable when the sample size is less than the number of model parameters [34]. Hu et al. [40] recently proposed a corrected BIC (CBIC) designed specifically for selecting the optimal value of K in a stochastic block model. They found that standard BIC may overestimate the true number of communities. CBIC adds an additional penalty to the log-likelihood, which may better estimate the optimal value of K . Biernacki et al. [14] proposed the integrated complete likelihood (ICL) to determine the optimal value of K and also found that standard BIC may overestimate K . Each of these limitations can be explored in future work to help possibly improve model performance.

Funding Information

This work was supported by grants 1R01DK131267-01 and 1R01GM141519 from the National Institutes of Health, 2210912 and 2113674 from the National Science Foundation, and AT-2030-20200401 from the Welch Foundation. NJD was supported by a research grant from the Foundation for Women’s Wellness. MLN was supported by National Institutes of Health Fellowship 1F32DK128975-01A1.

Conflict of Interest

The authors declare no potential conflict of interest.

Data Availability Statement

Whole genome metagenomic sequencing read data (FASTQ files) have been deposited onto the NIH Sequence Read Archive (SRA) under the BioProject number [NCBI]: PRJNA801448. Prior to depositing, all human-mapping reads were removed from the data. Simulated data, filtered real urinary microbiome abundance data used for analysis, and the related source code in R are available at <https://github.com/klutz920/Bayesian-SBM-MRF>. The *Les Misérables* data are publicly available in the `gsbm` library in R.

Orcid

<i>Kevin C. Lutz</i>	https://orcid.org/0000-0002-6687-0637
<i>Michael L. Neugent</i>	https://orcid.org/0000-0002-9863-9595
<i>Tejasv Bedi</i>	https://orcid.org/0000-0001-7532-4075
<i>Nicole J. De Nisco</i>	https://orcid.org/0000-0002-7670-5301
<i>Qiwei Li</i>	https://orcid.org/0000-0002-1020-3050

A Appendix of Supplementary Tables and Figures

Table 3: Available software for stochastic block models in R, Python, and C++ languages. Abbreviations: (i) Approach is either Bayesian (Bayes) or frequentist (Freq); (ii) Graph is either directed (D) or undirected (U); (iii) Data can be binary (B), discrete (P), or continuous (C); (iv) Companion publications for some of the packages are currently not available (NA).

Package	Approach	Graph	Data	Language	Repository	Publication
anocva	Freq	U	B,P,C	R	CRAN	[89]
BipartiteSBM	Bayes	U	B	Python/C++	GitHub	NA
blockmodeling	Freq	U	B,P,C	R	CRAN	[99]
blockmodels	Freq	D,U	B,P,C	R	CRAN	[55]
CommunityDetection	Freq	U	B	Python	GitHub	NA
dBlockmodeling	Freq	D,U	B,P,C	R	CRAN	[15]
dynSBM	Freq	U	B,P,C	R	CRAN	[65]
expSBM	Freq	D,U	B,C	R	CRAN	[78]
graphon	Bayes	U	B	R	CRAN	[73]
graph-tool	Bayes	D,U	B,P,C	Python	Online	[75]
greed	Bayes	D,U	B,P,C	R	CRAN	[21]
GREMLIN	Freq	D,U	B,P,C	R	CRAN	[8]
hergm	Bayes	D,U	B	R	CRAN	[81]
igraph	Freq	D,U	B,P,C	R	CRAN	[24]
missSBM	Freq	D,U	B	R	CRAN	[9]
MixeR	Bayes, Freq	U	B,P,C	R	CRAN	NA
MODE-NET	Freq	U	B	C++	Online	NA
noisySBM	Freq	D,U	C	R	CRAN	[79]
pysbm	Bayes, Freq	D,U	B,P,C	Python	GitHub	[30]
sbm	Freq	D,U	B,P,C	R	CRAN	NA
sbm_canonical_mcmc	Bayes	U	B	C++	GitHub	[95]
sbmr	Bayes	U	B,P	R	GitHub	NA
sbmSDP	Freq	U	B	R	CRAN	NA
SBMSplitMerge	Bayes	D,U	B,P,C	R	CRAN	[60]
SparseSBM	Freq	D,U	B	Python	GitHub	NA

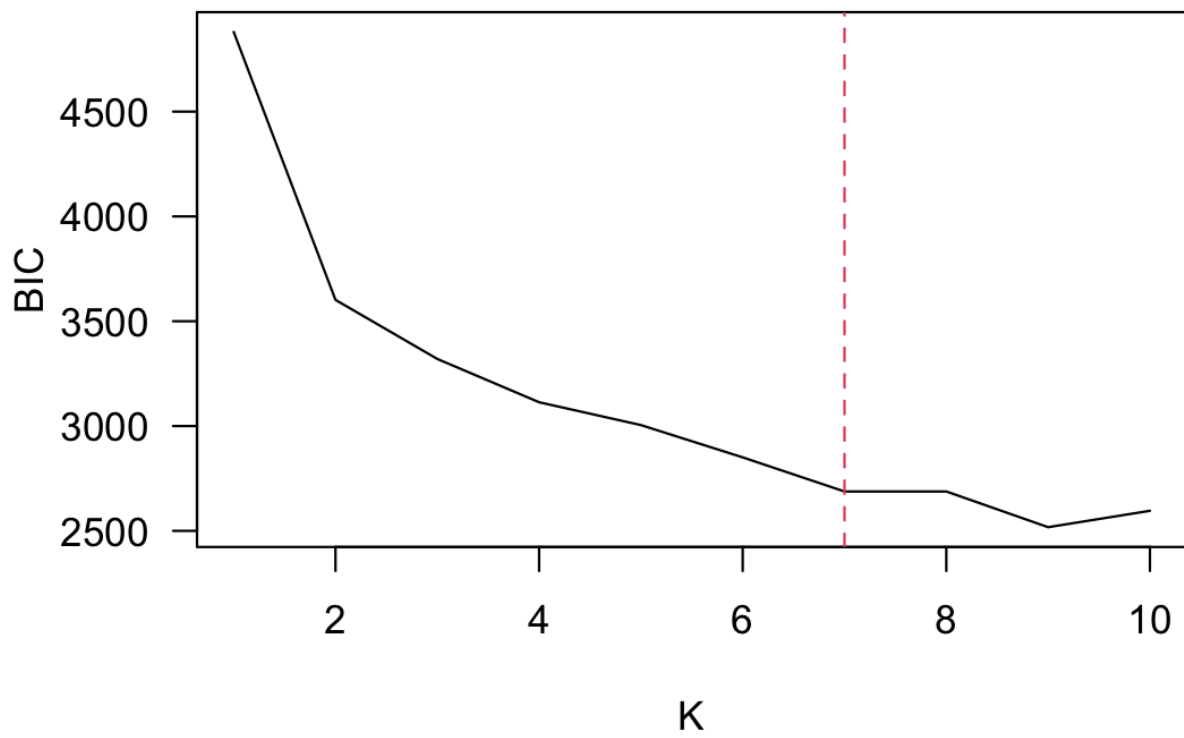


Figure 8: Elbow plot of BIC for the rUTI dataset by Bayesian-SBM-MRF ($f = 1$). The elbow is at $K = 7$ as indicated by the dashed red line.

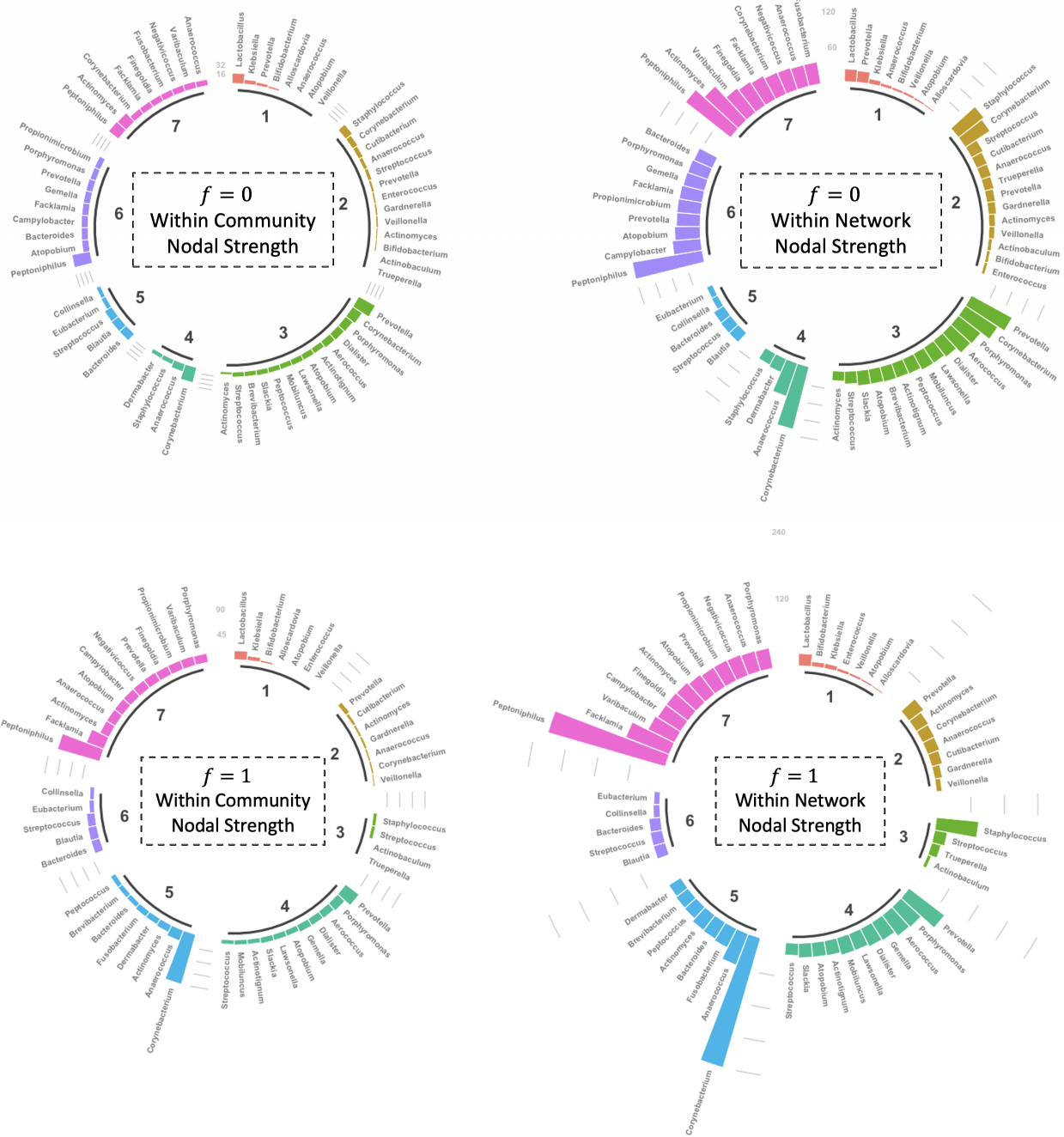


Figure 9: Circular bar plots of the nodal strength by genus within each community and within the entire network. The two top figures correspond to the standard Bayesian SBM ($f = 0$) indicating that no taxonomic tree data have been incorporated into the model; the two bottom figures correspond to Bayesian-SBM-MRF ($f = 1$) that incorporates taxonomic tree information.

Table 4: Online documentation for implementing available stochastic block model software packages. The year of the most recent software update is provided in the last column.

Package	URL	Updated
anocva	https://cran.r-project.org/web/packages/anocva/index.html	2023
BipartiteSBM	https://github.com/junipertcy	2020
blockmodeling	https://cran.r-project.org/web/packages/blockmodeling/index.html	2022
blockmodels	https://cran.r-project.org/web/packages/blockmodels/index.html	2021
CommunityDetection	https://github.com/Jonas1312/community-detection-in-graphs	2017
dBlockmodeling	https://cran.r-project.org/web/packages/dBlockmodeling/index.html	2020
dynSBM	https://cran.r-project.org/web/packages/dynsbm/index.html	2020
expSBM	https://cran.r-project.org/web/packages/expSBM/index.html	2019
graphon	https://cran.r-project.org/web/packages/graphon/index.html	2021
graph-tool	https://graph-tool.skewed.de	2017
greed	https://cran.r-project.org/web/packages/greed/index.html	2022
GREMLIN	https://cran.r-project.org/web/packages/gremlin/index.html	2021
hergm	https://cran.r-project.org/web/packages/hergm/index.html	2021
igraph	https://cran.r-project.org/web/packages/igraph/index.html	2023
missSBM	https://cran.r-project.org/web/packages/missSBM/index.html	2022
Mixer	https://rdrr.io/cran/mixer/	2018
MODE-NET	http://www.lps.ens.fr/~krzakala/MODE_NET/	2012
noisySBM	https://cran.r-project.org/web/packages/noisySBM/index.html	2020
pysbm	https://github.com/funket/pysbm/tree/master/pysbm	2019
sbm	https://cran.r-project.org/web/packages/sbm/index.html	2021
sbm_canonical_mcmc	https://github.com/jg-you/sbm_canonical_mcmc	2019
sbmr	https://github.com/tbilab/sbmr	2020
sbmSDP	https://cran.r-project.org/web/packages/sbmSDP/	2015
SBMSplitMerge	https://cran.r-project.org/web/packages/SBMSplitMerge/index.html	2020
SparseBM	https://github.com/gfrisch/sparsebm	2021

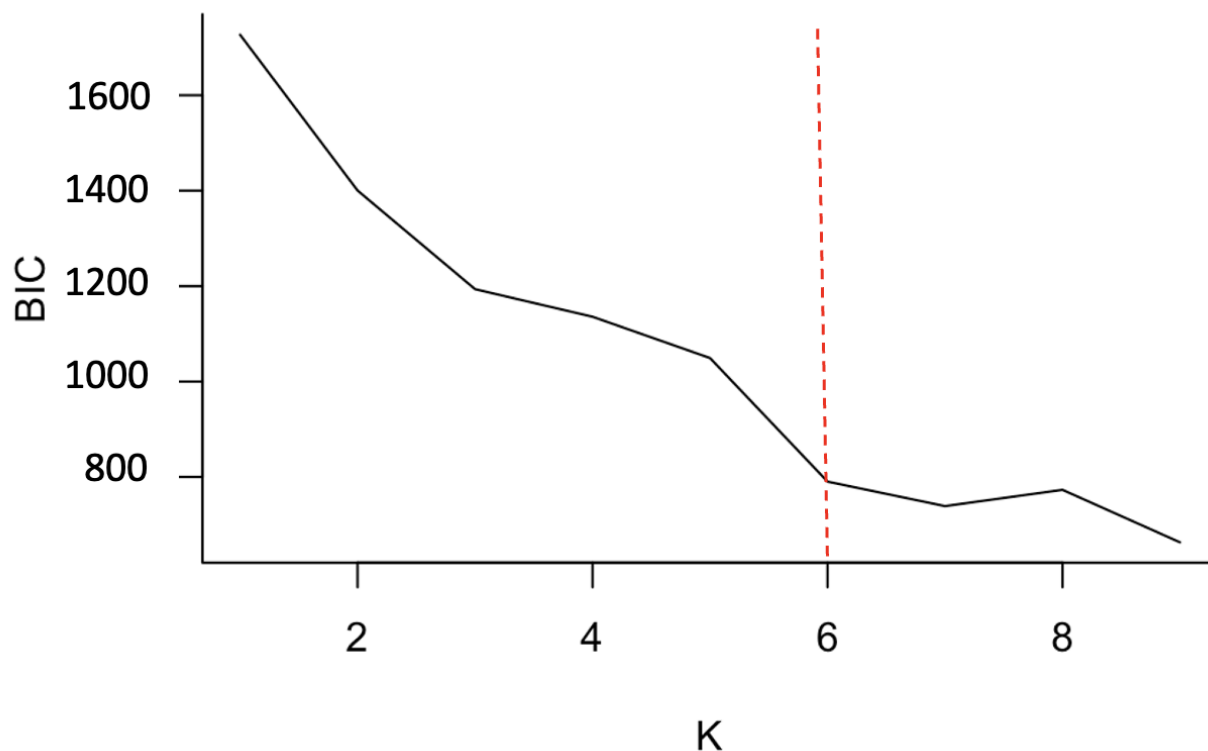


Figure 10: Elbow plot of BIC for the *Les Misérables* dataset by Bayesian-SBM-MRF ($f = 1$). The elbow is at $K = 6$ as indicated by the dashed red line.

References

- [1] Structure, function and diversity of the healthy human microbiome. *nature*, 486(7402):207–214, 2012.
- [2] Emmanuel Abbe, Afonso S Bandeira, and Georgina Hall. Exact recovery in the stochastic block model. *IEEE Transactions on information theory*, 62(1):471–487, 2015.
- [3] Roberto Daniel Aguinardo, Geoffrey Solano, Marc Jermaine Pontiveros, and Marilen Parungao Balolong. Namdata: A web-application for the network analysis of microbiome data. In *TENCON 2021-2021 IEEE Region 10 Conference (TENCON)*, pages 341–346. IEEE, 2021.
- [4] Christopher Aicher, Abigail Z Jacobs, and Aaron Clauset. Learning latent block structure in weighted networks. *Journal of Complex Networks*, 3(2):221–248, 2015.
- [5] John Aitchison. The statistical analysis of compositional data. *Journal of the Royal Statistical Society: Series B (Methodological)*, 44(2):139–160, 1982.
- [6] Rachael E Antwis, Sarah M Griffiths, Xavier A Harrison, Paz Aranega-Bou, Andres Arce, Aimee S Bettridge, Francesca L Brailsford, Alexandre de Menezes, Andrew Devaynes, Kristian M Forbes, et al. Fifty important research questions in microbial ecology. *FEMS Microbiology Ecology*, 93(5):fix044, 2017.
- [7] Michelle Badri, Zachary D Kurtz, Christian L Müller, and Richard Bonneau. Normalization methods for microbial abundance data strongly affect correlation estimates. *bioRxiv*, page 406264, 2018.
- [8] Avner Bar-Hen, Pierre Barbillon, and Sophie Donnet. Block models for generalized multipartite networks: Applications in ecology and ethnobiology. *Statistical Modelling*, page 1471082X20963254, 2020.
- [9] Pierre Barbillon, Julien Chiquet, and Timothée Tabouy. missbm: An r package for handling missing values in the stochastic block model. *arXiv preprint arXiv:1906.12201*, 2019.
- [10] Mathieu Bastian, Sebastien Heymann, and Mathieu Jacomy. Gephi: an open source software for exploring and manipulating networks. In *Proceedings of the international AAAI conference on web and social media*, volume 3, pages 361–362, 2009.
- [11] Yoav Benjamini and Yosef Hochberg. Controlling the false discovery rate: a practical and powerful approach to multiple testing. *Journal of the Royal statistical society: series B (Methodological)*, 57(1):289–300, 1995.
- [12] Julian Besag. Spatial interaction and the statistical analysis of lattice systems. *Journal of the Royal Statistical Society: Series B (Methodological)*, 36(2):192–225, 1974.
- [13] Anirban Bhar, Laurin Christopher Gierse, Alexander Meene, Haitao Wang, Claudia Korte, Theresa Schwaiger, Charlotte Schröder, Thomas C Mettenleiter, Tim Urich, Katharina Riedel, et al. Application of a maximal-clique based community detection algorithm to gut microbiome data reveals driver microbes during influenza a virus infection. *Frontiers in Microbiology*, 13:979320, 2022.
- [14] Christophe Biernacki, Gilles Celeux, and Gérard Govaert. Assessing a mixture model for clustering with the integrated completed likelihood. *IEEE transactions on pattern analysis and machine intelligence*, 22(7):719–725, 2000.
- [15] Michael Brusco, Patrick Doreian, and Douglas Steinley. Deterministic blockmodelling of signed and two-mode networks: A tutorial with software and psychological examples. *British Journal of Mathematical and Statistical Psychology*, 74(1):34–63, 2021.
- [16] Quy Cao, Xinxin Sun, Karun Rajesh, Naga Chalasani, Kayla Gelow, Barry Katz, Vijay H Shah, Arun J Sanyal, and Ekaterina Smirnova. Effects of rare microbiome taxa filtering on statistical analysis. *Frontiers in microbiology*, 11:607325, 2021.
- [17] Camilla Ceccarani, Claudio Foschi, Carola Parolin, Antonietta D’Antuono, Valeria Gaspari, Clarissa Consolandi, Luca Laghi, Tania Camboni, Beatrice Vitali, Marco Severgnini, et al. Diversity of vaginal microbiome and metabolome during genital infections. *Scientific reports*, 9(1):14095, 2019.
- [18] Y Erin Chen, Michael A Fischbach, and Yasmine Belkaid. Skin microbiota–host interactions. *Nature*, 553(7689):427–436, 2018.
- [19] Barry A Cipra. An introduction to the ising model. *The American Mathematical Monthly*, 94(10):937–959, 1987.

- [20] Peter Clifford. Markov random fields in statistics. *Disorder in physical systems: A volume in honour of John M. Hammersley*, pages 19–32, 1990.
- [21] Etienne Côme and Nicolas Jouvin. greed: An r package for model-based clustering by greedy maximization of the integrated classification likelihood. *arXiv preprint arXiv:2204.14063*, 2022.
- [22] Nora Connor, Albert Barberán, and Aaron Clauset. Using null models to infer microbial co-occurrence networks. *PloS one*, 12(5):e0176751, 2017.
- [23] Gregory W Corder and Dale I Foreman. *Nonparametric statistics: A step-by-step approach*. John Wiley & Sons, 2014.
- [24] Gabor Csardi, Tamas Nepusz, et al. The igraph software package for complex network research. *InterJournal, complex systems*, 1695(5):1–9, 2006.
- [25] Chad M Cullen, Kawalpreet K Aneja, Sinem Beyhan, Clara E Cho, Stephen Woloszynek, Matteo Convertino, Sophie J McCoy, Yanyan Zhang, Matthew Z Anderson, David Alvarez-Ponce, et al. Emerging priorities for microbiome research. *Frontiers in microbiology*, 11:136, 2020.
- [26] Miguel de Celis, Javier Duque, Domingo Marquina, Humbert Salvadó, Susana Serrano, Lucía Arregui, Antonio Santos, and Ignacio Belda. Niche differentiation drives microbial community assembly and succession in full-scale activated sludge bioreactors. *NPJ biofilms and microbiomes*, 8(1):1–6, 2022.
- [27] Courtney M Dunphy, Tarik C Gouhier, Nathaniel D Chu, and Steven V Vollmer. Structure and stability of the coral microbiome in space and time. *Scientific reports*, 9(1):1–13, 2019.
- [28] Joshua Faskowitz, Xiaoran Yan, Xi-Nian Zuo, and Olaf Sporns. Weighted stochastic block models of the human connectome across the life span. *Scientific reports*, 8(1):1–16, 2018.
- [29] Karoline Faust and Jeroen Raes. CoNet app: inference of biological association networks using Cytoscape. *F1000Research*, 5, 2016.
- [30] Thorben Funke and Till Becker. Stochastic block models: A comparison of variants and inference methods. *PloS one*, 14(4):e0215296, 2019.
- [31] Stuart Geman and Donald Geman. Stochastic relaxation, gibbs distributions, and the bayesian restoration of images. *IEEE Transactions on pattern analysis and machine intelligence*, (6):721–741, 1984.
- [32] Arsham Ghavasieh, Sebastiano Bontorin, Oriol Artime, Nina Verstraete, and Manlio De Domenico. Multi-scale statistical physics of the pan-viral interactome unravels the systemic nature of sars-cov-2 infections. *Communications Physics*, 4(1):1–13, 2021.
- [33] Guilherme Giovanini, Luciana RC Barros, Leonardo R Gama, Tharcisio C Tortelli Jr, and Alexandre F Ramos. A stochastic binary model for the regulation of gene expression to investigate responses to gene therapy. *Cancers*, 14(3):633, 2022.
- [34] Christophe Giraud. *Introduction to high-dimensional statistics*. CRC Press, 2021.
- [35] Jonas Halfvarson, Colin J Brislawn, Regina Lamendella, Yoshiki Vázquez-Baeza, William A Walters, Lisa M Bramer, Mauro D’amato, Ferdinando Bonfiglio, Daniel McDonald, Antonio Gonzalez, et al. Dynamics of the human gut microbiome in inflammatory bowel disease. *Nature Microbiology*, 2(5):1–7, 2017.
- [36] Caitlin V Hall, Anton Lord, Richard Betzel, Martha Zakrzewski, Lisa A Simms, Andrew Zalesky, Graham Radford-Smith, and Luca Cocchi. Co-existence of network architectures supporting the human gut microbiome. *Isience*, 22:380–391, 2019.
- [37] David Hevey. Network analysis: a brief overview and tutorial. *Health Psychology and Behavioral Medicine*, 6(1):301–328, 2018.
- [38] Peter D Hoff. *A first course in Bayesian statistical methods*, volume 580. Springer, 2009.
- [39] Paul W Holland, Kathryn Blackmond Laskey, and Samuel Leinhardt. Stochastic blockmodels: First steps. *Social networks*, 5(2):109–137, 1983.
- [40] Jianwei Hu, Hong Qin, Ting Yan, and Yunpeng Zhao. Corrected bayesian information criterion for stochastic block models. *Journal of the American Statistical Association*, 115(532):1771–1783, 2020.

- [41] Zongcheng Ji, Tian Xia, Mei Han, and Jing Xiao. A neural transition-based joint model for disease named entity recognition and normalization. In *Proceedings of the 59th Annual Meeting of the Association for Computational Linguistics and the 11th International Joint Conference on Natural Language Processing (Volume 1: Long Papers)*, pages 2819–2827, 2021.
- [42] Shuang Jiang, Guanghua Xiao, Andrew Y Koh, Yingfei Chen, Bo Yao, Qiwei Li, and Xiaowei Zhan. HARMONIES: A Hybrid Approach for Microbiome Networks Inference via Exploiting Sparsity. *Frontiers in Genetics*, 11:445, 2020.
- [43] Shuang Jiang, Quan Zhou, Xiaowei Zhan, and Qiwei Li. Bayessmiles: Bayesian segmentation modeling for longitudinal epidemiological studies. *MedRxiv*, 2020.
- [44] Shuang Jiang, Guanghua Xiao, Andrew Y Koh, Jiwoong Kim, Qiwei Li, and Xiaowei Zhan. A bayesian zero-inflated negative binomial regression model for the integrative analysis of microbiome data. *Biostatistics*, 22(3):522–540, 2021.
- [45] Fredrik H Karlsson, Valentina Tremaroli, Intawat Nookaew, Göran Bergström, Carl Johan Behre, Björn Fagerberg, Jens Nielsen, and Fredrik Bäckhed. Gut metagenome in European women with normal, impaired and diabetic glucose control. *Nature*, 498(7452):99–103, 2013.
- [46] Brian Karrer and Mark EJ Newman. Stochastic blockmodels and community structure in networks. *Physical review E*, 83(1):016107, 2011.
- [47] Robert E Kass and Adrian E Raftery. Bayes factors. *Journal of the american statistical association*, 90(430):773–795, 1995.
- [48] Donald Ervin Knuth. *The Stanford GraphBase: a platform for combinatorial computing*, volume 1. AcM Press New York, 1993.
- [49] Matthew D Koslovsky, Kristi L Hoffman, Carrie R Daniel, and Marina Vannucci. A bayesian model of microbiome data for simultaneous identification of covariate associations and prediction of phenotypic outcomes. *The Annals of Applied Statistics*, 14(3):1471–1492, 2020.
- [50] Bhusan K Kuntal, Pranjal Chandrakar, Sudipta Sadhu, and Sharmila S Mande. ‘netshift’: a methodology for understanding ‘driver microbes’ from healthy and disease microbiome datasets. *The ISME journal*, 13(2):442–454, 2019.
- [51] Pierre Latouche, Etienne Birmelé, and Christophe Ambroise. Overlapping stochastic block models with application to the french political blogosphere. *The Annals of Applied Statistics*, 5(1):309–336, 2011.
- [52] Robert Leaman and Zhiyong Lu. Taggerone: joint named entity recognition and normalization with semi-markov models. *Bioinformatics*, 32(18):2839–2846, 2016.
- [53] Joshua Lederberg and Alexa T McCray. Ome sweetomics—a genealogical treasury of words. *The scientist*, 15(7):8–8, 2001.
- [54] Clement Lee and Darren J Wilkinson. A review of stochastic block models and extensions for graph clustering. *Applied Network Science*, 4(1):1–50, 2019.
- [55] Jean-Benoist Leger. Blockmodels: A r-package for estimating in latent block model and stochastic block model, with various probability functions, with or without covariates. *arXiv preprint arXiv:1602.07587*, 2016.
- [56] Emilie Lejal, Julien Chiquet, Julie Aubert, Stephane Robin, A Estrada-Peña, Olivier Rue, Cédric Midoux, Mahendra Mariadassou, Xavier Bailly, Arnaud Cougoul, et al. Temporal patterns in ixodes ricinus microbial communities: an insight into tick-borne microbe interactions. *Microbiome*, 9(1):1–20, 2021.
- [57] Huazhang Li, Yaotian Wang, Guofen Yan, Yinge Sun, Seiji Tanabe, Chang-Chia Liu, Mark S Quigg, and Tingting Zhang. A bayesian state-space approach to mapping directional brain networks. *Journal of the American Statistical Association*, 116(536):1637–1647, 2021.
- [58] Xiaoni Liu. Focus: Microbiome: Microbiome. *The Yale Journal of Biology and Medicine*, 89(3):275, 2016.
- [59] Yinxia Lou, Yue Zhang, Tao Qian, Fei Li, Shufeng Xiong, and Donghong Ji. A transition-based joint model for disease named entity recognition and normalization. *Bioinformatics*, 33(15):2363–2371, 2017.
- [60] Matthew Ludkin. Inference for a generalised stochastic block model with unknown number of blocks and non-conjugate edge models. *Computational Statistics & Data Analysis*, 152:107051, 2020.

- [61] Kevin C Lutz, Shuang Jiang, Michael L Neugent, Nicole J De Nisco, Xiaowei Zhan, and Qiwei Li. A survey of statistical methods for microbiome data analysis. *Frontiers in Applied Mathematics and Statistics*, page 55, 2022.
- [62] Julian R Marchesi, Bas E Dutilh, Neil Hall, Wilbert HM Peters, Rian Roelofs, Annemarie Boleij, and Harold Tjalsma. Towards the human colorectal cancer microbiome. *PLoS One*, 6(5):e20447, 2011.
- [63] Julian R Marchesi, David H Adams, Francesca Fava, Gerben DA Hermes, Gideon M Hirschfield, Georgina Hold, Mohammed Nabil Quraishi, James Kinross, Hauke Smidt, Kieran M Tuohy, et al. The gut microbiota and host health: a new clinical frontier. *Gut*, 65(2):330–339, 2016.
- [64] Cameron Martino, James T Morton, Clarisse A Marotz, Luke R Thompson, Anupriya Tripathi, Rob Knight, and Karsten Zengler. A novel sparse compositional technique reveals microbial perturbations. *MSystems*, 4(1):10–1128, 2019.
- [65] Catherine Matias and Vincent Miele. Statistical clustering of temporal networks through a dynamic stochastic block model. *Journal of the Royal Statistical Society: Series B (Statistical Methodology)*, 79(4):1119–1141, 2017.
- [66] Aaron F McDaid, Thomas Brendan Murphy, Nial Friel, and Neil J Hurley. Improved bayesian inference for the stochastic block model with application to large networks. *Computational Statistics & Data Analysis*, 60:12–31, 2013.
- [67] Paul D McNicholas. *Mixture model-based classification*. Chapman and Hall/CRC, 2016.
- [68] Michael L Neugent, Ashwani Kumar, Neha V Hulyalkar, Kevin C Lutz, Vivian H Nguyen, Jorge L Fuentes, Cong Zhang, Amber Nguyen, Belle M Sharon, Amy Kuprasertkul, et al. Recurrent urinary tract infection and estrogen shape the taxonomic ecology and function of the postmenopausal urogenital microbiome. *Cell Reports Medicine*, page 100753, 2022.
- [69] Victoria KY Ng and Robert A Cribbie. The gamma generalized linear model, log transformation, and the robust yuen-welch test for analyzing group means with skewed and heteroscedastic data. *Communications in Statistics-Simulation and Computation*, 48(8):2269–2286, 2019.
- [70] Laetitia Nouedoui and Pierre Latouche. Bayesian non parametric inference of discrete valued networks. In *21-th European Symposium on Artificial Neural Networks, Computational Intelligence and Machine Learning (ESANN 2013)*, pages 291–296, 2013.
- [71] Krzysztof Nowicki and Tom A B Snijders. Estimation and prediction for stochastic blockstructures. *Journal of the American statistical association*, 96(455):1077–1087, 2001.
- [72] Santiago Olivella, Tyler Pratt, and Kosuke Imai. Dynamic stochastic blockmodel regression for network data: Application to international militarized conflicts. *Journal of the American Statistical Association*, pages 1–14, 2022.
- [73] Peter Orbanz and Daniel M Roy. Bayesian models of graphs, arrays and other exchangeable random structures. *IEEE transactions on pattern analysis and machine intelligence*, 37(2):437–461, 2014.
- [74] Asli I Özen and David W Ussery. Defining the pseudomonas genus: where do we draw the line with azotobacter? *Microbial ecology*, 63:239–248, 2012.
- [75] Tiago P Peixoto. Bayesian stochastic blockmodeling. *Advances in network clustering and blockmodeling*, pages 289–332, 2019.
- [76] Thomas P Quinn, Ionas Erb, Greg Gloor, Cedric Notredame, Mark F Richardson, and Tamsyn M Crowley. A field guide for the compositional analysis of any-omics data. *GigaScience*, 8(9):giz107, 2019.
- [77] William M Rand. Objective criteria for the evaluation of clustering methods. *Journal of the American Statistical association*, 66(336):846–850, 1971.
- [78] Riccardo Rastelli and Michael Fop. A dynamic stochastic blockmodel for interaction lengths. *arXiv preprint arXiv:1901.09828*, 2019.
- [79] Tabea Rebafka, Etienne Roquain, and Fanny Villers. Graph inference with clustering and false discovery rate control. *arXiv preprint arXiv:1907.10176*, 2019.
- [80] Gideon Schwarz. Estimating the dimension of a model. *The annals of statistics*, pages 461–464, 1978.

- [81] Michael Schweinberger and Pamela Luna. Hergm: Hierarchical exponential-family random graph models. *Journal of Statistical Software*, 85:1–39, 2018.
- [82] Elena Shipitsyna, Annika Roos, Raluca Datcu, Anders Hallén, Hans Fredlund, Jørgen S Jensen, Lars Engstrand, and Magnus Unemo. Composition of the vaginal microbiota in women of reproductive age—sensitive and specific molecular diagnosis of bacterial vaginosis is possible? *PloS one*, 8(4):e60670, 2013.
- [83] Andrew B Shreiner, John Y Kao, and Vincent B Young. The gut microbiome in health and in disease. *Current opinion in gastroenterology*, 31(1):69, 2015.
- [84] Anjali Silva, Steven J Rothstein, Paul D McNicholas, and Sanjeena Subedi. A multivariate poisson-log normal mixture model for clustering transcriptome sequencing data. *BMC bioinformatics*, 20(1):1–11, 2019.
- [85] Natalie Stanley, Thomas Bonacci, Roland Kwitt, Marc Niethammer, and Peter J Mucha. Stochastic block models with multiple continuous attributes. *Applied Network Science*, 4(1):1–22, 2019.
- [86] Caroline M Tucker, Marc W Cadotte, Silvia B Carvalho, T Jonathan Davies, Simon Ferrier, Susanne A Fritz, Rich Grenyer, Matthew R Helmus, Lanna S Jin, Arne O Mooers, et al. A guide to phylogenetic metrics for conservation, community ecology and macroecology. *Biological Reviews*, 92(2):698–715, 2017.
- [87] Salih Tuna and Mahesan Niranjana. Classification with binary gene expressions. *Journal of Biomedical Science and Engineering*, 2(6):390–399, 2009.
- [88] Peter J Turnbaugh, Ruth E Ley, Micah Hamady, Claire M Fraser-Liggett, Rob Knight, and Jeffrey I Gordon. The human microbiome project. *Nature*, 449(7164):804–810, 2007.
- [89] Maciel C Vidal, João R Sato, Joana B Balardin, Daniel Y Takahashi, and André Fujita. Anocva in r: a software to compare clusters between groups and its application to the study of autism spectrum disorder. *Frontiers in neuroscience*, 11:16, 2017.
- [90] Dewan F Wahid and Elkafi Hassini. A literature review on correlation clustering: Cross-disciplinary taxonomy with bibliometric analysis. In *Operations Research Forum*, volume 3, pages 1–42. Springer, 2022.
- [91] Stefanie Widder, Irene Görzer, Benjamin Friedel, Nina Rahimi, Stefan Schwarz, Peter Jaksch, Sylvia Knapp, and Elisabeth Puchhammer-Stöckl. Metagenomic sequencing reveals time, host, and body compartment-specific viral dynamics after lung transplantation. *Microbiome*, 10(1):1–13, 2022.
- [92] Mi-Young Won, Linda B Oyama, Stephen J Courtney, Christopher J Creevey, and Sharon A Huws. Can rumen bacteria communicate to each other? *Microbiome*, 8(1):1–8, 2020.
- [93] Zhenxing Xu, Yoko Masuda, Xueding Wang, Natsumi Ushijima, Yutaka Shiratori, Keishi Senoo, and Hideomi Itoh. Genome-based taxonomic rearrangement of the order geobacterales including the description of *geomonas azotofigans* sp. nov. and *geomonas diazotrophica* sp. nov. *Frontiers in Microbiology*, 12:737531, 2021.
- [94] Grace Yoon, Irina Gaynanova, and Christian L Müller. Microbial networks in SPRING-Semi-parametric rank-based correlation and partial correlation estimation for quantitative microbiome data. *Frontiers in Genetics*, 10:516, 2019.
- [95] Jean-Gabriel Young, Patrick Desrosiers, Laurent Hébert-Dufresne, Edward Laurence, and Louis J Dubé. Finite-size analysis of the detectability limit of the stochastic block model. *Physical Review E*, 95(6):062304, 2017.
- [96] Jin-Zhu Yu and Hiba Baroud. Modeling uncertain and dynamic interdependencies of infrastructure systems using stochastic block models. *ASCE-ASME Journal of Risk and Uncertainty in Engineering Systems, Part B: Mechanical Engineering*, 6(2):020906, 2020.
- [97] Lisha Yu, William H Woodall, and Kwok-Leung Tsui. Detecting node propensity changes in the dynamic degree corrected stochastic block model. *Social Networks*, 54:209–227, 2018.
- [98] Sendong Zhao, Ting Liu, Sicheng Zhao, and Fei Wang. A neural multi-task learning framework to jointly model medical named entity recognition and normalization. In *Proceedings of the AAAI Conference on Artificial Intelligence*, volume 33, pages 817–824, 2019.
- [99] Aleš Žiberna. Generalized blockmodeling of valued networks. *Social networks*, 29(1):105–126, 2007.